AD-A204 886 TRANSVERSE WAKE POTENTIALS FOR WIDE RADIAL LINES(U) 1/1
SCIENCE APPLICATIONS INTERNATIONAL CORP ALBUQUERQUE NM
B B GODFREY 07 MAR 88 N60921-85-C-0044

UNCLASSIFIED F/G 20/7 NL

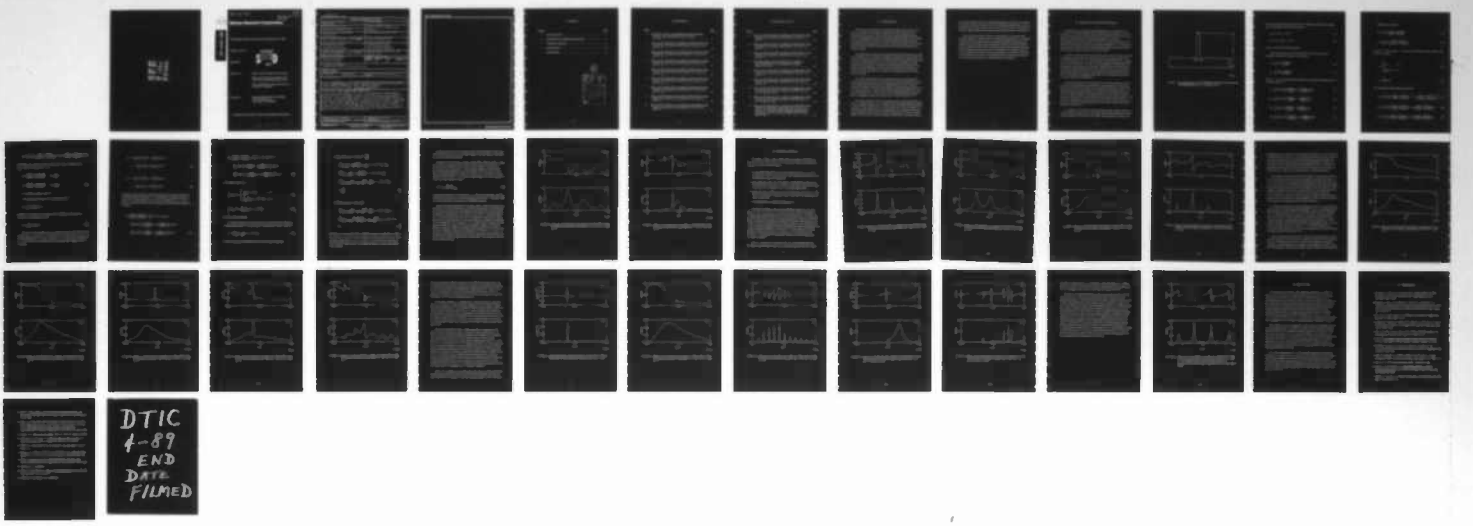

DTIC
4-89
END
DATE
FILMED

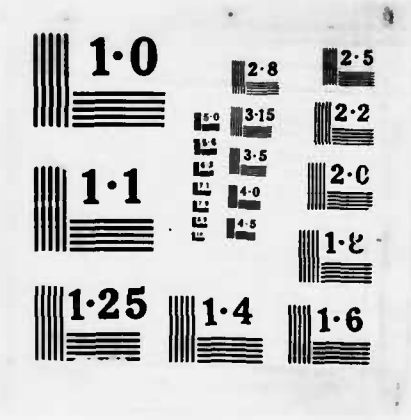
1·0
1·1
1·25
1·4
1·6
2·8
3·15
3·5
4·0
4·5
2·5
2·2
2·0
1·8

DTIC FILE COPY

(4)

MRC/ABQ-R-1046
Copy 123

Mission Research Corporation

TRANSVERSE WAKE POTENTIALS FOR WIDE RADIAL LINES

Brendan B. Godfrey

DTIC
ELECTE
FEB 2 8 1989
S D
D

March 1988

Sponsored by: Defense Advanced Research Projects Agency

Monitored by Naval Surface Weapons Center
under Contract N60921-85-C-0044 to SAIC

Science Applications International Corporation
Subcontract 15-860022-79

Prepared by: MISSION RESEARCH CORPORATION
1720 Randolph Road, SE.
Albuquerque, NM 87106-4245

APPROVED FOR PUBLIC RELEASE/UNLIMITED DISTRIBUTION

'89 2 27 194

UNCLASSIFIED

SECURITY CLASSIFICATION OF THIS PAGE

REPORT DOCUMENTATION PAGE

1a. REPORT SECURITY CLASSIFICATION UNCLASSIFIED	1b. RESTRICTIVE MARKINGS
2a. SECURITY CLASSIFICATION AUTHORITY	3 DISTRIBUTION/AVAILABILITY OF REPORT Approved for public release/unlimited distribution.
2b. DECLASSIFICATION/DOWNGRADING SCHEOULE	
4. PERFORMING ORGANIZATION REPORT NUMBER(S) MRC/ABQ-R-1046	5. MONITORING ORGANIZATION REPORT NUMBER(S)
6a. NAME OF PERFORMING ORGANIZATION Mission Research Corporation 6b. OFFICE SYMBOL (*If applicable*)	7a. NAME OF MONITORING ORGANIZATION Naval Surface Weapons Center
6c. ADDRESS (*City, State, and ZIP Code*) 1720 Randolph Road, SE Albuquerque, NM 87106-4245	7b. ADDRESS (*City, State, and ZIP Code*) 10901 New Hampshire Avenue Silver Spring, MD 20903-5000
8a. NAME OF FUNDING/SPONSORING ORGANIZATION Defense Advanced Research Projects Agency 8b OFFICE SYMBOL (*If applicable*)	9. PROCUREMENT INSTRUMENT IDENTIFICATION NUMBER N60921-85-C-0044
8c. ADDRESS (*City, State, and ZIP Code*) 1400 Wilson Boulevard Arlington, VA 22209	10. SOURCE OF FUNDING NUMBERS PROGRAM ELEMENT NO. / PROJECT NO / TASK NO / WORK UNIT ACCESSION NO
11. TITLE (*Include Security Classification*) TRANSVERSE WAKE POTENTIALS FOR WIDE RADIAL LINES	
12. PERSONAL AUTHOR(S) Godfrey, Brendan B.	
13a. TYPE OF REPORT / 13b. TIME COVERED FROM _____ TO _____ / 14. DATE OF REPORT (*Year, Month, Day*) 880307 / 15. PAGE COUNT	
16. SUPPLEMENTARY NOTATION	

17 COSATI CODES		
FIELD	GROUP	SUB-GROUP

18. SUBJECT TERMS (*Continue on reverse if necessary and identify by block number*)
Compact Induction Accelerators; ELECTRON ACCELERATORS;
High Current Electron Beams;
Beam Breakup Instability. (cont)

19. ABSTRACT (*Continue on reverse if necessary and identify by block number*)

The transverse wake potential for a radial line terminated by a lumped impedance is derived analytically for arbitrary line width. Using these formulas, the wake potential is evaluated numerically for parameters relevant to high current, electron beam, induction accelerators. The transverse wake potential scales as the line width divided by the square of the drift tube radius for narrow lines, in agreement with earlier studies. However, the potential becomes roughly independent of line width and varies only with the reciprocal of the drift tube radius for widths somewhat greater than the radius. Several additional resonances arising for wide lines do complicate the scaling. Nonetheless, it appears that wide, high voltage radial lines may reduce beam breakup and image displacement instability growth significantly for compact accelerator designs.

Keywords:)

20. DISTRIBUTION/AVAILABILITY OF ABSTRACT ☐ UNCLASSIFIED/UNLIMITED ☐ SAME AS RPT. ☐ OTIC USERS	21. ABSTRACT SECURITY CLASSIFICATION UNCLASSIFIED
22a. NAME OF RESPONSIBLE INDIVIDUAL	22b. TELEPHONE (*Include Area Code*) / 22c. OFFICE SYMBOL

DD FORM 1473, 84 MAR 83 APR edition may be used until exhausted. All other editions are obsolete.

SECURITY CLASSIFICATION OF THIS PAGE
UNCLASSIFIED

CONTENTS

DTIC COPY INSPECTED 1

Accesion For
NTIS CRA&I
DTIC TAB
Unannounced
Justification
By
Distribution /
Availability Codes
Dist | Avail and / or Special
A-1

ILLUSTRATIONS

ILLUSTRATIONS (Cont'd)

1.0 INTRODUCTION

The beam breakup instability is a serious issue for high current, electron beam, induction accelerators. The instability degraded beam quality somewhat in the Experimental Test Accelerator (ETA) at Lawrence Livermore National Laboratory (LLNL).[1] Knowledge gained from ETA experiments allowed developers of the Advanced Test Accelerator (ATA) to optimize the induction modules for reduced instability.[2] Nonetheless, beam breakup growth was so great in this long accelerator that ion-focused transport had to be added to minimize current loss.[3,4] Even now, emittance growth remains a problem.

The beam breakup instability arises from the interaction of the electron beam with its own transverse ($m = 1$) wake fields, reflected by discontinuities in the accelerator drift tube wall.[5] Standing waves excited in the radial feed lines of the acceleration modules are the major source of beam breakup in high current induction accelerators, although reflections from pumping ports, diagnostics, and the like should not be ignored. The image displacement instability, which is caused by interruption of the beam image current in the drift tube wall,[6] can be viewed as the low frequency limit of the beam breakup instability.

The beam breakup instability is particularly worrisome for recently proposed compact induction accelerators, such as the Spiral Line Induction Accelerator,[7] because the instability growth rate increases with decreasing drift tube radius. The actual variation of the growth rate with drift tube radius, b, and acceleration gap width, d, has been uncertain, however. A careful study of ATA gap impedances predicts d/b^2 scaling but is valid only for $d/b < 1$.[2] On the other hand, the image displacement instability growth rate is known to scale as d/b^2 only for $d/b < 1$, and as $1/b$ for $d/b > 1$.[8,9]

This report extends the radial line impedance analysis to arbitrary gap width and arbitrary instability frequency. Our principal finding is encouraging. Generally speaking, the transverse wake potential due to a radial line scales only as $1/b$ for wide gaps. The combination of high voltage per gap, accommodated by the $1/b$ scaling, and heavy gap damping appears to reduce beam breakup growth significantly for compact accelerator designs.[10] The variation of transverse impedance with gap width is not simple, however,

because electromagnetic modes in the radial line shift greatly in frequency and strength as d increases. Another interesting result is that potentially dangerous modes can exist at frequencies up to the TM_{1n} cutoff and not just up to the TE_{1n} cutoff, as one might have supposed. Weakly damped modes trapped in the mouth of the line also were discovered.

The outline of this report is as follows. The derivation of the transverse wake potential equations for a radial line with a lumped impedance termination is summarized in Chapter 2. Then, numerical solutions are compared in different limiting cases with published results from earlier papers to establish the validity of the extensive algebra involved. Chapter 3 contains a wealth of numerical results demonstrating the scaling of the wake potential with gap width, depth, and termination load. Although variations about the standard ATA radial line model are emphasized, a few shallow, weakly loaded, wall indentations also are treated to shed additional light on high-Q modes trapped in cavity entrances and small ports. Conclusions are drawn in Chapter 4.

2.0 DERIVATION OF THE WAKE POTENTIAL

The wake potential is defined as the time-integrated force on a particle in an accelerator due to the electromagnetic fields of another particle preceding it by a time t. Thus, the wake potential is the temporal Green's function for the net force of the beam acting upon itself, evaluated in the paraxial and long betatron-wavelength approximations. Here we are interested only in the $m = 1$ transverse component of the wake potential, which gives rise to the beam breakup instability. The $m = 0$ longitudinal wake potential, on the other hand, characterizes beam loading of the acceleration gaps. It also causes axial beam bunching in, for instance, klystrons.

Formally, the wake potential associated with a gap in the drift tube wall is obtained analytically by matching the vector Green's function for electromagnetic fields in the cavity behind the gap to the vector Green's function for the smooth drift tube, using the current of the first particle as the source term and integrating the resulting fields along the trajectory of the second particle following it. This approach works in practice only for geometries sufficiently simple that the cavity Green's function can be expanded in known normal modes. Otherwise, the wake potential must be determined numerically with multidimensional electromagnetic field solvers.[10,11] The relative merits of various techniques are discussed in Reference 12.

The model considered for the radial feed line in an induction accelerator (ATA, in particular) is a simple radial line terminated by a lumped impedance Z_s. See Figure 1, which shows the drift tube of radius b and the radial line of width d and depth R. The magnitude of the terminating impedance is normalized to the impedance of free space. Even in this simple configuration the algebra required to obtain the wake potential is substantial. However, since it roughly follows the analyses used in earlier studies,[2,9,13] the calculation is presented here only in outline form. The reader is referred particularly to Reference 13, which derives the longitudinal and transverse potentials for radial lines of arbitrary width with $Z_s = 0$.

For simplicity all calculations are performed in the frequency domain. Further, the beam particles are assumed to move at the speed of light, a good approximation in most electron accelerators. The fields of a point charge traveling axially in the smooth drift

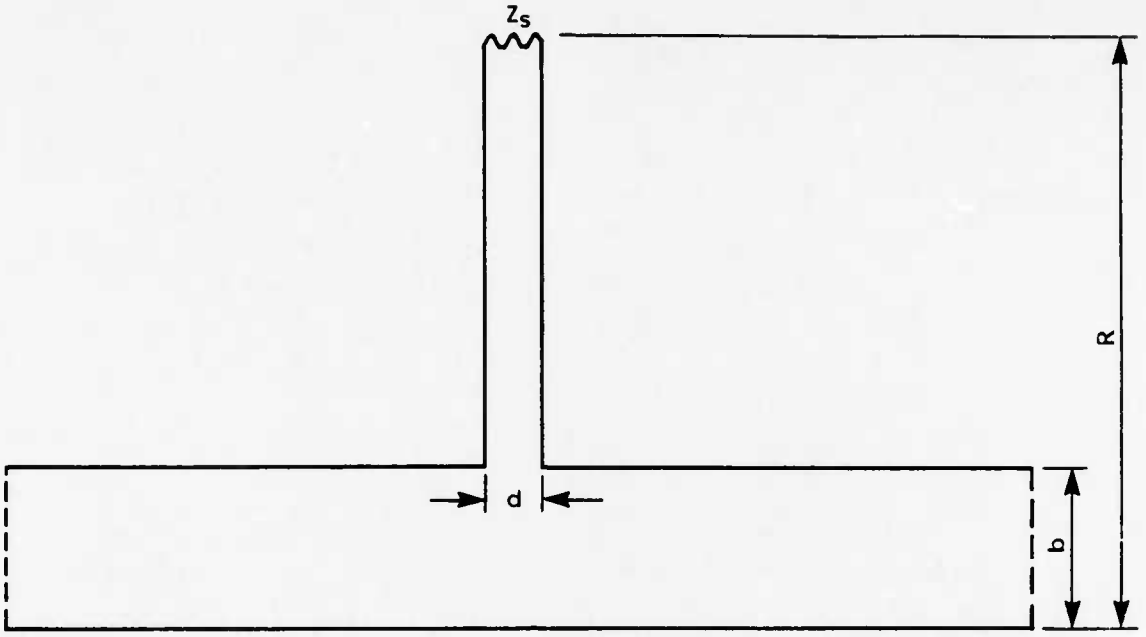

FIGURE 1. IDEALIZED RADIAL LINE GEOMETRY, HERE WITH THE NOMINAL ATA DIMENSIONS OF $R/b = 3.6$ AND $d/b = 0.34$.

tube are, in this limit, purely transverse. The $m = 1$ fields for a particle of unit charge and unit displacement from the axis are given by

$$E_r = B_\theta = \left(b^{-2} + r^{-2}\right) e^{i\omega z} \tag{1}$$

$$E_\theta = -B_r = i\left(b^{-2} - r^{-2}\right) e^{i\omega z} \tag{2}$$

where ω is the standard frequency variable.

The vacuum fields in both the drift tube and the radial line are expressed conveniently in TM and TE modes. In the drift tube,

$$E_z = \frac{1}{2\pi}\int dk E_k \frac{J_1(q_k r)}{J_1(q_k b)} e^{ikz} \tag{3}$$

$$B_z = \frac{1}{2\pi}\int dk B_k \frac{J_1(q_k r)}{q_k J_1'(q_k b)} e^{ikz} \tag{4}$$

with $q_k^2 = \omega^2 - k^2$. The transverse field components are obtained from Equations 3 and 4 in the usual fashion.[14]

$$E_r = \frac{1}{2\pi}\int dk\, q_k^{-2}\left[ik\frac{q_k J_1'(q_k r)}{J_1(q_k b)}E_k - \frac{\omega}{r}\frac{J_1(q_k r)}{q_k J_1'(q_k b)}B_k\right] e^{ikz} \tag{5}$$

$$E_\theta = \frac{1}{2\pi}\int dk\, q_k^{-2}\left[-\frac{k}{r}\frac{J_1(q_k r)}{J_1(q_k b)}E_k - i\omega\frac{J_1'(q_k r)}{J_1'(q_k b)}B_k\right] e^{ikz} \tag{6}$$

$$B_r = \frac{1}{2\pi}\int dk\, q_k^{-2}\left[ik\frac{J_1'(q_k r)}{J_1'(q_k b)}B_k + \frac{\omega}{r}\frac{J_1(q_k r)}{J_1(q_k b)}E_k\right] e^{ikz} \tag{7}$$

$$B_\theta = \frac{1}{2\pi}\int dk\, q_k^{-2}\left[-\frac{k}{r}\frac{J_1(q_k r)}{q_k J_1'(q_k b)}B_k + i\omega\frac{q_k J_1'(q_k r)}{J_1(q_k b)}E_k\right] e^{ikz} \tag{8}$$

Likewise, in the radial line,

$$E_z = \sum_n E_n f_n \frac{Y_1(q_n r) - \beta_E J_1(q_n r)}{Y_1(q_n b) - \beta_E J_1(q_n b)} \tag{9}$$

$$B_z = \sum_n B_n g_n \frac{Y_1(q_n r) - \beta_B J_1(q_n r)}{q_n \left(Y_1'(q_n b) - \beta_B J_1'(q_n b)\right)} \tag{10}$$

with $q_n^2 = \omega^2 - k_n^2$. Note that $k_n = n\pi/d$, with n a non-negative integer, is distinct from k, which is continuous.

$$f_n = \begin{cases} \dfrac{1}{\sqrt{d}}\,, & n = 0 \\ \sqrt{\dfrac{2}{d}} \cos k_n z\,, & n > 0 \end{cases} \tag{11}$$

$$g_n = \sqrt{\frac{2}{d}}\, \sin k_n z \tag{12}$$

The corresponding transverse field components are

$$E_r = \sum_n q_n^{-2} \left[f_n' q_n \frac{Y_1'(q_n r) - \beta_E J_1'(q_n r)}{Y_1(q_n b) - \beta_E J_1(q_n b)} E_n - \frac{\omega}{r} g_n \frac{Y_1(q_n r) - \beta_B J_1(q_n r)}{q_n \left(Y_1'(q_n b) - \beta_B J_1'(q_n b)\right)} B_n \right] \tag{13}$$

$$E_\theta = \sum_n q_n^{-2} \left[f_n' \frac{i}{r} \frac{Y_1(q_n r) - \beta_E J_1(q_n r)}{Y_1(q_n b) - \beta_E J_1(q_n b)} E_n - i\omega g_n \frac{Y_1'(q_n r) - \beta_B J_1'(q_n r)}{Y_1'(q_n b) - \beta_B J_1'(q_n b)} B_n \right] \tag{14}$$

$$B_r = \sum_n q_n^{-2} \left[g_n' \frac{Y_1'(q_n r) - \beta_B J_1'(q_n r)}{Y_1'(q_n b) - \beta_B J_1'(q_n b)} B_n + \frac{\omega}{r} f_n \frac{Y_1(q_n r) - \beta_E J_1(q_n r)}{Y_1(q_n b) - \beta_E J_1(q_n b)} E_n \right] \tag{15}$$

$$B_\theta = \sum_n q_n^{-2} \left[g'_n \frac{i}{r} \frac{Y_1(q_n r) - \beta_B J_1(q_n r)}{q_n \left(Y'_1(q_n b) - \beta_B J'_1(q_n b) \right)} B_n + i\omega f_n \, q_n \frac{Y'_1(q_n r) - \beta_E J'_1(q_n r)}{Y_1(q_n b) - \beta_E J_1(q_n b)} E_n \right] \quad (16)$$

The coefficients β_E and β_B are chosen so that $E_z/B_\theta = Z_s$ for the TM mode, and $E_\theta/B_z = Z_s$ for the TE mode, at $r = R$.

$$\beta_E = \frac{Y_1(q_n R) - \eta_E q_n Y'_1(q_n R)}{J_1(q_n R) - \eta_E q_n J'_1(q_n R)} \quad ; \quad \eta_E \equiv \frac{i\omega}{q_n^2} Z_s \quad (17)$$

$$\beta_B = \frac{Y_1(q_n R) - \eta_B q_n Y'_1(q_n R)}{J_1(q_n R) - \eta_B q_n J'_1(q_n R)} \quad ; \quad \eta_B \equiv \frac{i\omega}{q_n^2} Z_s^{-1} \quad (18)$$

J_1 and Y_1 are Bessel functions of order 1.[15]

The wake potential is related to E_z in the drift tube by[2,12]

$$W = \frac{1}{i\omega} \int dt \frac{1}{r} \frac{\partial}{\partial r} r E_z e^{-i\omega z} \quad (19)$$

evaluated at the trajectory of the second particle. If we assume $r \ll b$, this can be written on the basis of Equation 3 as[16]

$$W = \frac{2}{i\omega b} \int_0^d dz E_k e^{-i\omega z} \quad (20)$$

E_θ and B_r in the two regions are continuous across the mouth of the radial line and zero elsewhere on the surface $r = b$. Therefore, we can relate E_k and B_k to E_n and B_n by multiplying Equations 6, 7, 14, and 15, evaluated at $r = b$, by $\exp(-ikz)$, integrating over all z, and combining the corresponding results. The particle fields, Equation 2, do not contribute.

$$E_k = kb\sum_n q_n^{-2}\left[-i\frac{k_n}{b}E_n - i\omega B_n\right]\int_0^d dz g_n e^{-ikz}$$

$$+\omega b\sum_n q_n^{-2}\left[k_n B_n + \frac{\omega}{b}E_n\right]\int_0^d dz f_n e^{-ikz} \tag{21}$$

$$B_k = i\omega\sum_n q_n^{-2}\left[-i\frac{k_n}{b}E_n - i\omega B_n\right]\int_0^d dz g_n e^{-ikz}$$

$$+ik\sum_n q_n^{-2}\left[k_n B_n + \frac{\omega}{b}E_n\right]\int_0^d dz f_n e^{-ikz} \tag{22}$$

E_r and B_θ, on the other hand, are continuous across the mouth of the radial line but unspecified elsewhere on the surface $r = b$. Consequently, we multiply Equations 1, 5, and 13 by f_n, multiply Equations 1, 8, and 16 by g_n, integrate over $0 < z < d$, and combine corresponding results to obtain a second pair of relations between fields in the two regions.

$$E_n q_n \frac{Y_1'(q_n b) - \beta_E J_1'(q_n b)}{Y_1(q_n b) - \beta_E J_1(q_n b)} = \frac{2}{b}\int_0^d dz\left(-i\omega f_n + k_n g_n\right)e^{i\omega z}$$

$$-\frac{i\omega}{2\pi}\int dk q_k^{-2}\left[-\frac{k}{b}\frac{J_1(q_k b)}{q_k J_1'(q_k b)}B_k + i\omega q_k\frac{J_1'(q_k b)}{J_1(q_k b)}E_k\right]\int_0^d dz f_n e^{ikz}$$

$$+\frac{k_n}{2\pi}\int dk q_k^{-2}\left[ikq_k\frac{J_1'(q_k b)}{J_1(q_k b)}E_k - \frac{\omega}{b}\frac{J_1(q_k b)}{q_k J_1'(q_k b)}B_k\right]\int_0^d dz g_n e^{ikz} \tag{23}$$

$$B_n \frac{Y_1(q_n b) - \beta_B J_1(q_n b)}{q_n \left(Y_1'(q_n b) - \beta_B J_1'(q_n b)\right)} = \frac{2}{b}\int_0^d dz\,(-\omega g_n + ik_n f_n)\,e^{i\omega z}$$

$$- \frac{\omega b}{2\pi}\int dk q_k^{-2}\left[ikq_k \frac{J_1'(q_k b)}{J_1(q_k b)}E_k - \frac{\omega}{b}\frac{J_1(q_k b)}{q_k J_1'(q_k b)}B_k\right]\int_0^d dz g_n e^{ikz}$$

$$+ \frac{ik_n b}{2\pi}\int dk q_k^{-2}\left[-\frac{k}{b}\frac{J_1(q_k b)}{q_k J_1'(q_k b)}B_k + i\omega q_k \frac{J_1'(q_k b)}{J_1(q_k b)}E_k\right]\int_0^d dz f_n e^{ikz} \tag{24}$$

The integrals are given by

$$\int_0^d dz f_n e^{-ikz} = \begin{cases} \frac{1}{\sqrt{d}}\frac{1}{ik}\left[1 - e^{-ikd}\right], & n = 0 \\ \sqrt{\frac{2}{d}}\frac{ik}{k_n^2 - k^2}\left[1 - (-1)^n e^{-ikd}\right], & n > 0 \end{cases} \tag{25}$$

$$\int_0^d dz g_n e^{-ikz} = \sqrt{\frac{2}{d}}\frac{k_n}{k_n^2 - k^2}\left[1 - (-1)^n e^{-ikd}\right] \tag{26}$$

and their complex conjugates.

The desired expression for the wake potential is obtained after much algebra by combining Equations 20–24 and performing the k integrations by contour methods.[2,13]

$$W = \frac{16}{b}\frac{b}{d}\sum_n E_n \frac{\epsilon_n}{q_n^2 b^2}\left[1 - (-1)^n \cos\omega d\right] \tag{27}$$

where E_n and B_n, now renormalized, are given by the system of equations,

$$E_n \left[\frac{\pi}{2} J_1(q_n b)\left(Y_1(q_n b) - \beta_E J_1(q_n b)\right)\right]^{-1} \frac{\omega^2 b^2}{q_n^2 b^2}$$

$$- \frac{4b}{d} \sum_{j,m} \frac{\chi_{E,j} b\, \omega^2 b^2}{(\chi_{E,j}^2 b^2 + k_n^2 b^2)(\chi_{E,j}^2 b^2 + k_m^2 b^2)} \left[1 - (-1)^n e^{-\chi_{E,j} d}\right] \epsilon_m E_m$$

$$+ \frac{4b}{d} \sum_{j,m} \frac{1}{\chi_{B,j} b (q_{B,j}^2 b^2 - 1)} \frac{\omega^2 b^2}{q_n^2 b^2} \frac{\omega^2 b^2}{q_m^2 b^2} \left[1 - (-1)^n e^{-\chi_{B,j} d}\right] \epsilon_m E_m$$

$$- \frac{4b}{d} \sum_{j,m} \frac{k_m b}{\chi_{B,j} b (\chi_{B,j}^2 b^2 + k_m^2 b^2)} \frac{q_{B,j}^2 b^2}{q_{B,j}^2 b^2 - 1} \frac{\omega^2 b^2}{q_n^2 b^2} \left[1 - (-1)^n e^{-\chi_{B,j} d}\right] B_m$$

$$= -\frac{\omega^2 b^2}{q_n^2 b^2} \tag{28}$$

$$B_n \left[\frac{\pi}{2} J_1'(q_n b)\left(Y_1'(q_n b) - \beta_B J_1'(q_n b)\right)\right]^{-1}$$

$$- \frac{4b}{d} \sum_{j,m} \frac{k_m b}{\chi_{B,j} b (\chi_{B,j}^2 b^2 + k_m^2 b^2)} \frac{q_{B,j}^2 b^2}{q_{B,j}^2 b^2 - 1} \frac{\omega^2 b^2}{q_m^2 b^2} \left[1 - (-1)^n e^{-\chi_{B,j} d}\right] E_m$$

$$+ \frac{4b}{d} \sum_{j,m} \frac{k_m b\, k_n b\, q_{B,j}^2 b^2}{\chi_{B,j} b (\chi_{B,j}^2 b^2 + k_m^2 b^2)(\chi_{B,j}^2 b^2 + k_n^2 b^2)} \frac{q_{B,j}^2 b^2}{q_{B,j}^2 b^2 - 1} \left[1 - (-1)^n e^{-\chi_{B,j} d}\right] B_m$$

$$= 0 \tag{29}$$

The sums on m are over even or odd non-negative integers only, depending on whether n is even or odd. ϵ_m is $\frac{1}{2}$ for $m = 0$ and 1 otherwise. $q_{E,j}$ and $q_{B,j}$ are the zeroes of $J_1(qb)$ and $J_1'(qb)$, respectively; $\chi_j^2 = q_j^2 - \omega^2$. When $\chi_j^2 < 0$, i.e., for drift tube modes above cutoff, choose the negative branch of the square root function to assure only outgoing waves at infinity.

We also have derived the wake potential from a somewhat different representation of the fields, based on E_z and E_θ, and slightly different matching conditions. Equivalent formulas were obtained, as expected.

Equations 27–29 are solved numerically using the BBU computer program, written for this purpose. Keeping ten terms in each of the sums typically is sufficient for a relative accuracy of better than 10^{-5}. The two complex matrices, n even and odd, representing Equations 28 and 29 are inverted using the LINPACK routine CGEFS.[17] Wake potentials from BBU can be written to a file for use in the accelerator transport computer program BALFFT.[10] Alternatively, dominant peaks in the wake potential can be fit to the single resonance model,[2,5]

$$W \approx \frac{\omega_0^3 Z_\perp / Q}{\omega^2 - \omega_0^2 - i\omega\,\omega_0/Q} \tag{30}$$

for comparison with theory. In Equation 30 ω_0, $Z_\perp$, and Q are the frequency, transverse impedance, and quality factor of the resonant mode in the radial line. A 1024-point BBU calculation requires about one minute on a CRAY-XMP computer.

Before surveying the dependence of the wake potential on radial line parameters, we demonstrate the accuracy of the BBU code and the analysis leading to it by comparing our numerical results with those of References 2 and 18. Figure 2 is the wake potential (multiplied by b) from BBU for $d/b = 0.34$, $R/b = 3.6$, and $Z_s = 2$. The plot extends to $\omega b/c = 3.83$, the TM cutoff in the drift tube. $W \cdot b$ generally is much smaller at higher frequencies. The wake potential in its usual units of ohm/cm is obtained by multiplying by 30 and dividing by b in cm. Because $d/b < 1$, we expect Figure 2b to agree well with Figure 7 of Reference 2, which it does. When making the comparison, note that the Reference 2 figure has a different normalization and extends only to 1.84, the TE cutoff. Our Figure 3 represents vastly different parameters, $d/b = 0.05$, $R/b = 1.1$, and $Z_s = 0$. Agreement with Figure 6 of Reference 18 is excellent. Elsewhere, results from BBU and the time-domain computer program ANDY were compared.[10] They agreed to within the accuracy of the latter code.

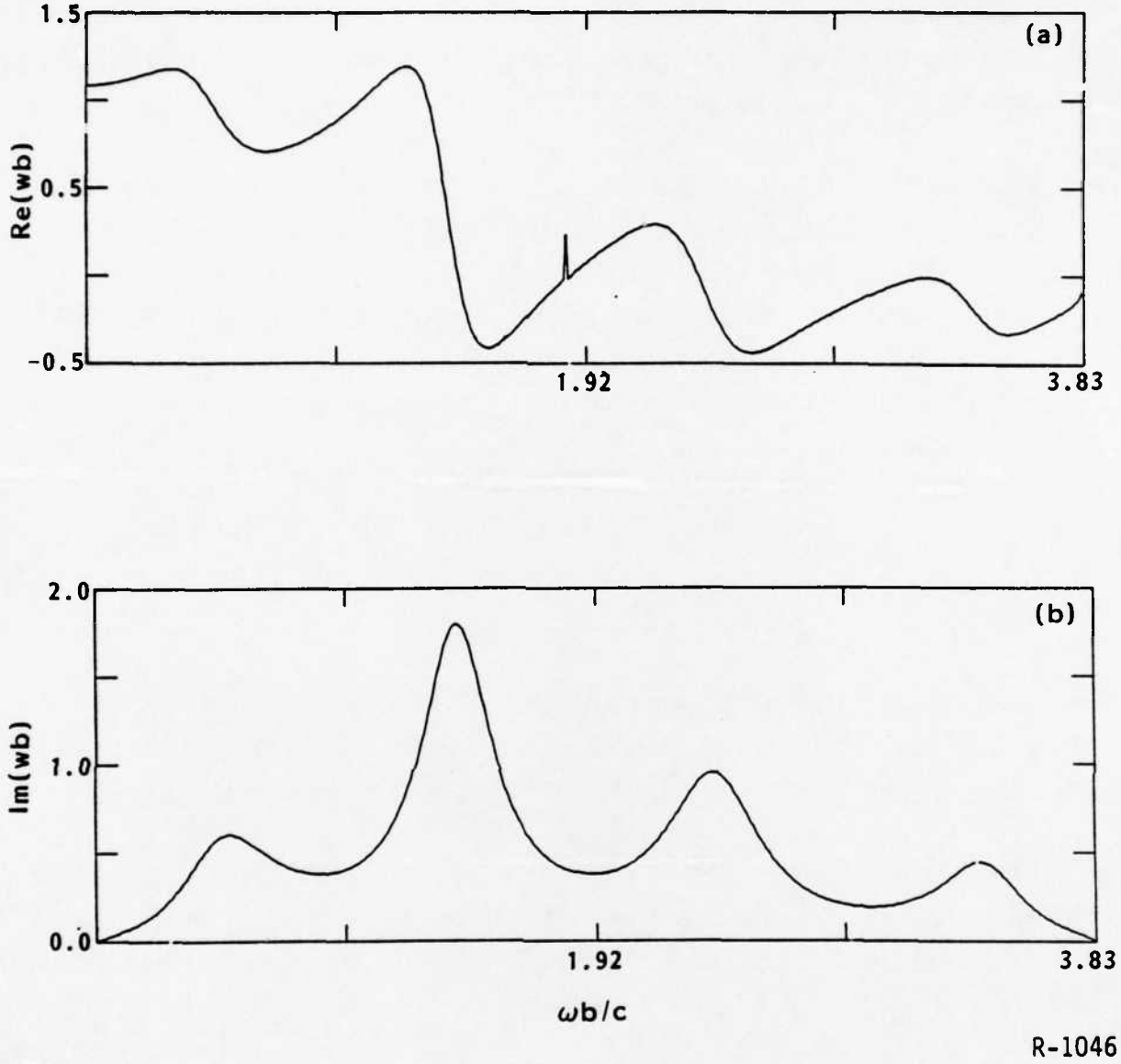

FIGURE 2. REAL (a) AND IMAGINARY (b) PARTS OF NORMALIZED WAKE POTENTIAL FOR RADIAL LINE WITH $R/b = 3.6$, $d/b = 0.34$, AND $Z_s = 2$.

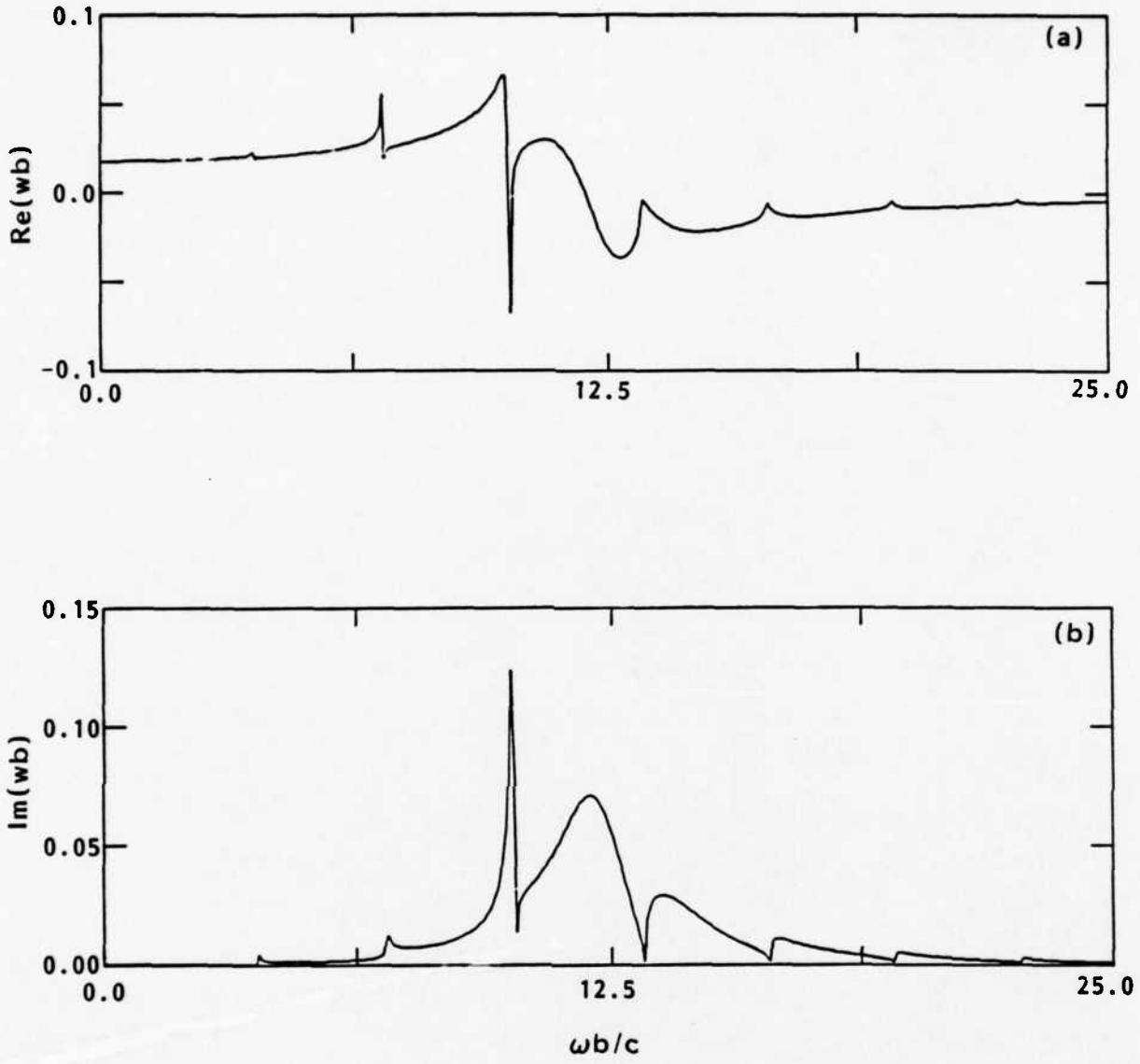

FIGURE 3. REAL (a) AND IMAGINARY (b) PARTS OF NORMALIZED WAKE POTENTIAL FOR RADIAL LINE WITH $R/b = 1.1$, $d/b = 0.05$, AND $Z_s = 0$.

3.0 NUMERICAL RESULTS

This section is largely a survey of BBU results for parameters centered about nominal ATA values: $d/b = 0.34$, $R/b = 3.6$, and $Z_s \approx 2$–3. The survey provides the basis for a number of useful observations.

1. The qualitative scaling of W with d and b switches from d/b^2 to $1/b$ as d/b is increased above unity. Consequently, wide, high voltage lines should result in less instability than narrow, low voltage lines.

2. The quantitative scaling of W with large d/b is complicated by the presence of additional modes in the radial line. Weakly damped modes trapped in the mouth of the radial line also appear for $d/b \approx 1$ and certain larger values.

3. Dangerous modes in radial lines can occur at any frequency up to the $m = 1$ TM cutoff of the wave guide. Typically, the most serious modes have frequencies just below the TE cutoff.

4. The wake potential is minimized by choosing $Z_s \approx 1$.

We begin by varying the line termination impedance. Figures 4, 5, 6, 2, and 7 depict $W \cdot b$ for $Z_s = 0.1, 0.5, 1.0, 2.0$, and 10.0. Z_s of zero or infinity corresponds to vanishing of the tangential electric field or its normal derivative at $r = R$. There is no energy dissipation below the TE cutoff in these two limits, and $Im(W \cdot b)$ is identically zero there. Resonance frequencies are well approximated by the mode frequencies of a pill-box cavity with corresponding radial boundary condition. As Z_s is moved toward unity, the resonant frequencies are relatively unchanged while mode damping grows. The minimum transverse impedance is achieved for $Z_s \approx 1$, where modes are so heavily damped that they become indistinct. Although a $Z_s = 1$ line termination is not equivalent to a transmission line radiating into free space, the corresponding wake potentials are similar.[19]

Since $Z_s = 1$ appears to be optimal, we next vary d/b while keeping the line termination impedance fixed at that value. R/b remains equal to 3.6 for now. Wake

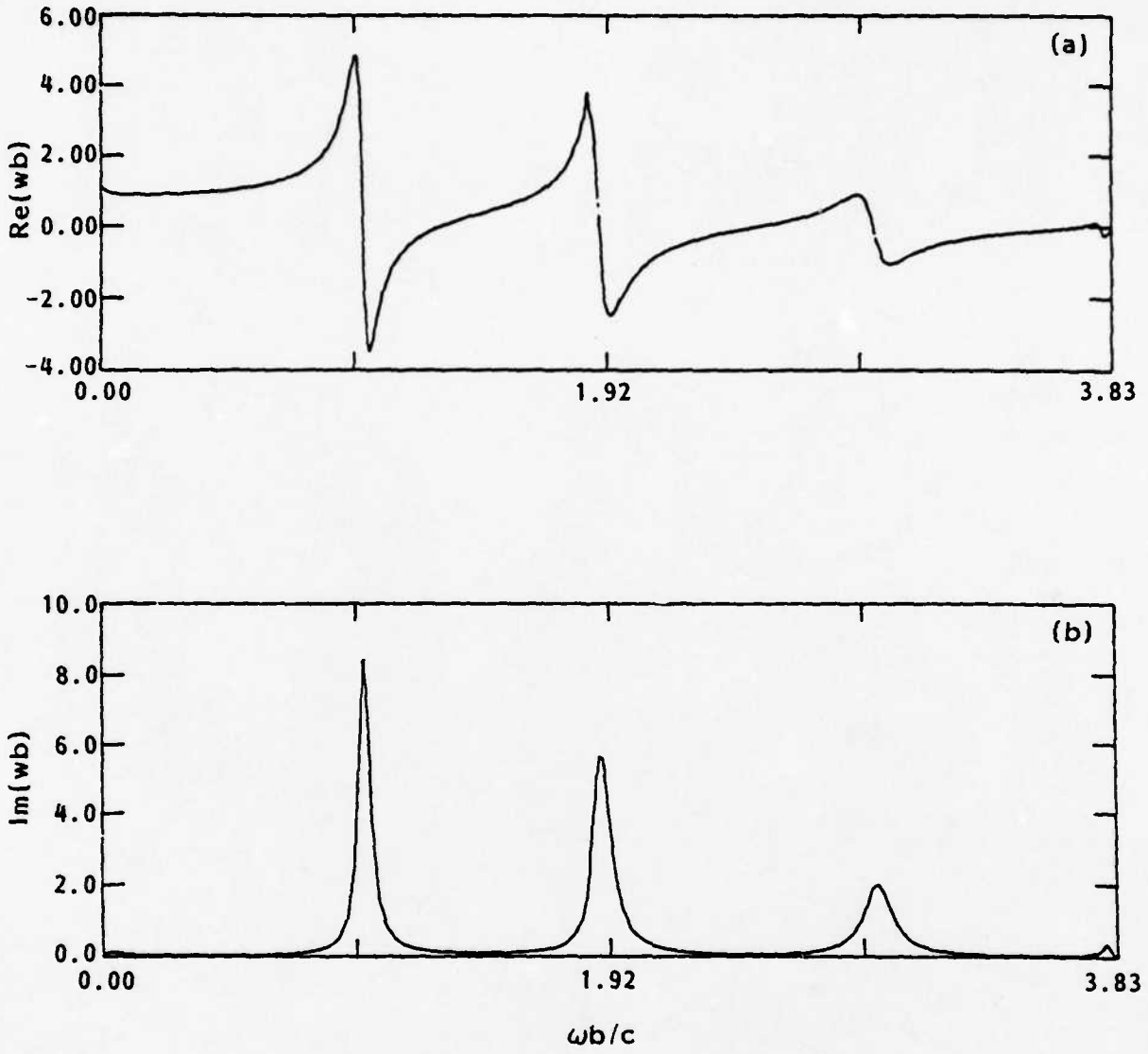

FIGURE 4. REAL (a) AND IMAGINARY (b) PARTS OF NORMALIZED WAKE POTENTIAL FOR RADIAL LINE WITH $R/b = 3.6$, $d/b = 0.34$, AND $Z_s = 0.1$.

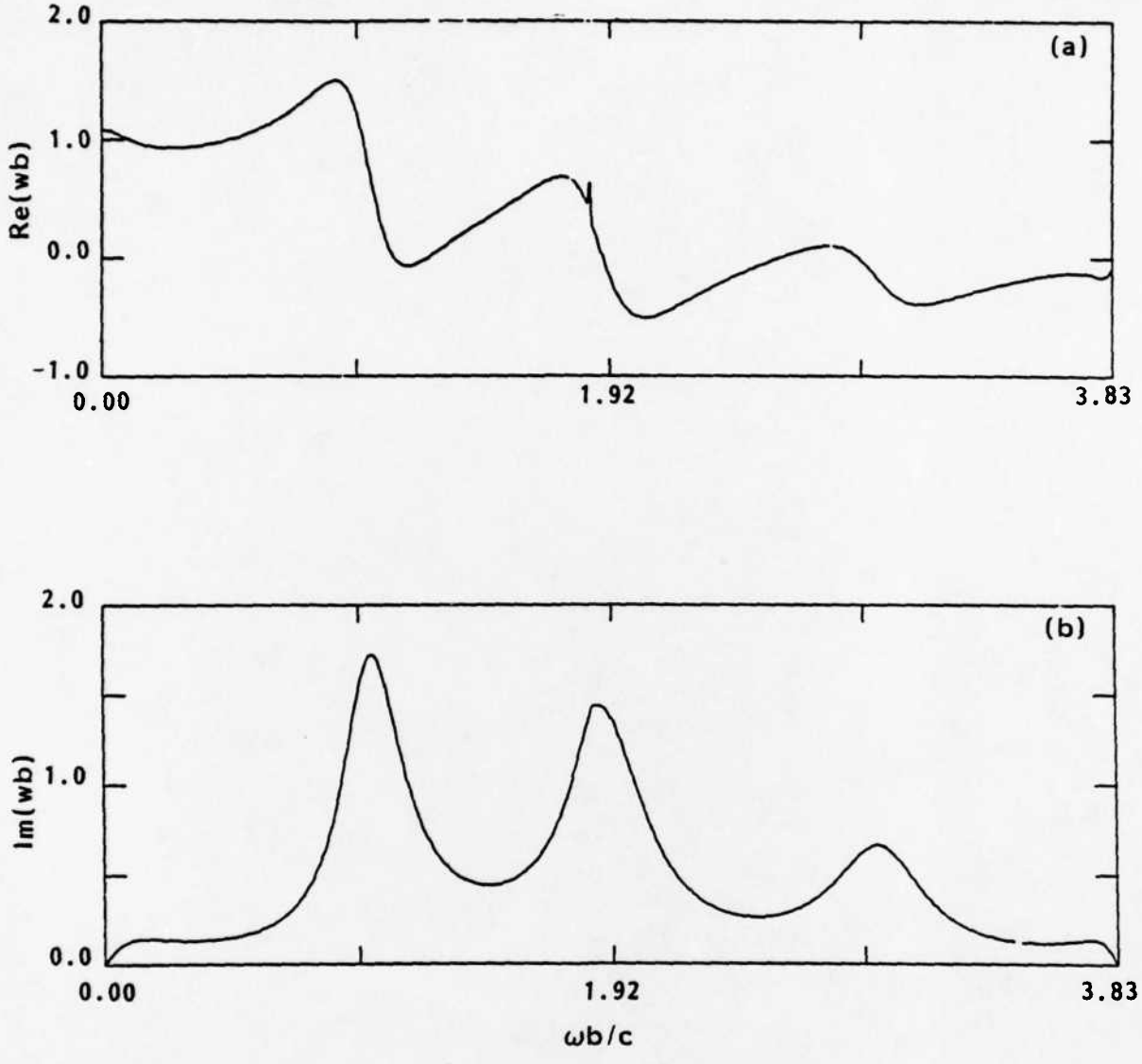

FIGURE 5. REAL (a) AND IMAGINARY (b) PARTS OF NORMALIZED WAKE POTENTIAL FOR RADIAL LINE WITH $R/b = 3.6$, $d/b = 0.34$, AND $Z_s = 0.5$.

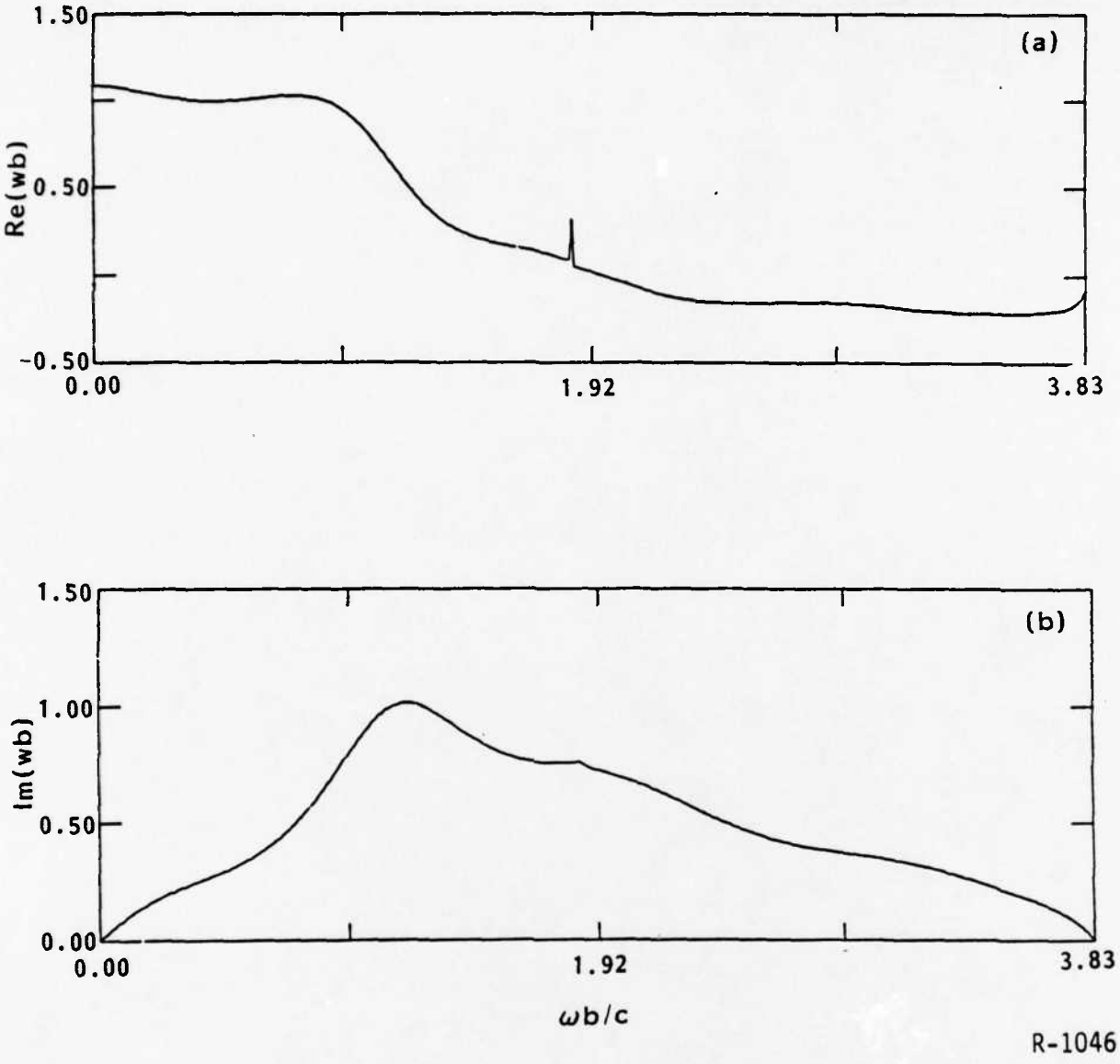

FIGURE 6. REAL (a) AND IMAGINARY (b) PARTS OF NORMALIZED WAKE POTENTIAL FOR RADIAL LINE WITH $R/b = 3.6$, $d/b = 0.34$, AND $Z_s = 1.0$.

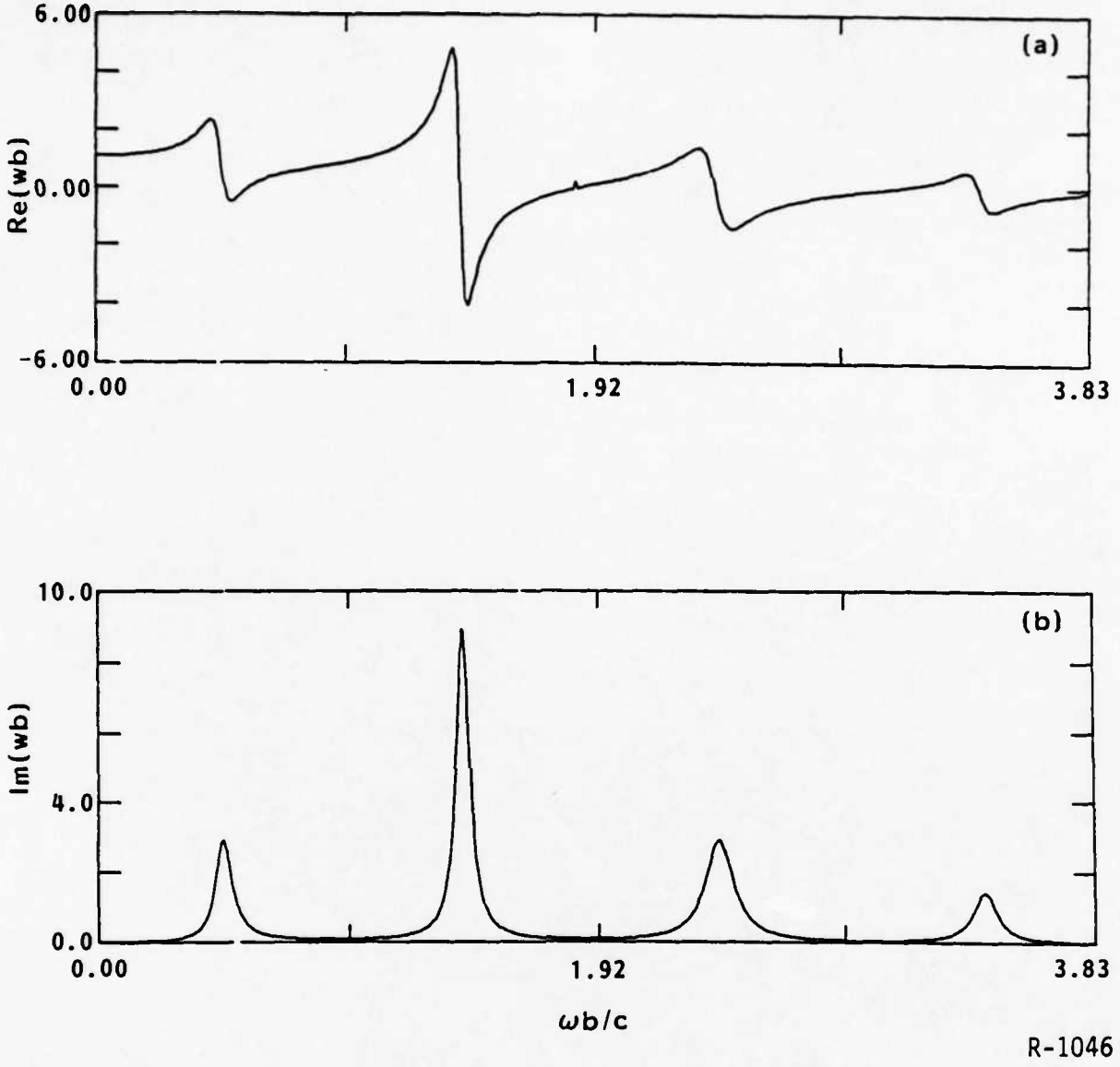

FIGURE 7. REAL (a) AND IMAGINARY (b) PARTS OF NORMALIZED WAKE POTENTIAL FOR RADIAL LINE WITH $R/b = 3.6$, $d/b = 0.34$, AND $Z_s = 10.0$.

potentials for $d/b = 0.1, 0.5, 1.0, 2.0$, and 5.0 are shown in Figures 8, 9, 10, 11, and 12. See also Figure 6 for $d/b = 0.34$. $W \cdot b$ is nearly constant in shape for $d/b \leq 0.5$ but increase in magnitude linearly as d/b. This corroborates the small d/b scaling of Reference 2. Even without the poorly resolved narrow mode dominating $Re(W \cdot b)$ in Figure 10, a departure from linear scaling is beginning to be evident for $d/b = 1.0$. The $Im(W \cdot b)$, although similar in shape between $d/b = 0.5$ and 1.0, increases only by a factor of 1.6. The narrow mode in Figure 10a is discussed further in a subsequent paragraph.

Still another new feature arises for $d/b = 2.0$, Figure 11. The prominent mode near $\omega b/c = 1.6$ is the lowest frequency wave in the radial line with axially varying E_z, i.e., $n = 1$ in Equations 27–29. By analogy with a metallic pill-box cavity, such modes occur for $\omega b/c > \pi b/d$. As will be more apparent from later figures, the new resonance happens to lie in the frequency range where transverse impedances tend to be large. The mode is dangerous, therefore. If the resonance is ignored, however, the continuing trend of ever weaker variation of $W \cdot b$ with d/b is evident. The trend continues in Figure 12, $d/b = 5.0$, despite the presence of several new modes. Although resonances appear and disappear as d/b is increased, the average magnitude of the wake potential remains more or less constant. This is particularly evident at low frequencies.

The lessened dependence of the wake potential on d/b for $d/b > 1$ has at least two causes. Just as in the image displacement instability,[6,8] the $m = 1$ electromagnetic fields causing the beam breakup instability are concentrated near the corners of the gap for $d/b > 1$. (Specifically, fields vary as rapidly as $x^{-1/3}$, where x is the distance from a corner.[20]) As a result, increasing d/b does not enhance the total force on the beam as much for d/b large. A second ameliorating factor is the transit-time effect. A beam particle traversing a sufficiently wide gap samples a range of phases of the $m = 1$ forces, which tend to cancel as a result. The term $[1 - (-1)^n \cos \omega d]b/d$ represents the transit-time effect in Equation 27. It first has a strong influence on the wake potential at frequencies near the TE cutoff for $d/b \approx 1.7$.

Before investigating the scaling of $W \cdot b$ with R/b, we remark further on the sharp resonance appearing in Figure 10a and, to a lesser extent, other plots. The resonance is due to a wave localized to the mouth of the radial line. Physically, it is somewhat analogous to an electromagnetic wave trapped in a short dielectric liner inside a metal tube. Its impedance is small, because its effective volume is limited. On the other hand,

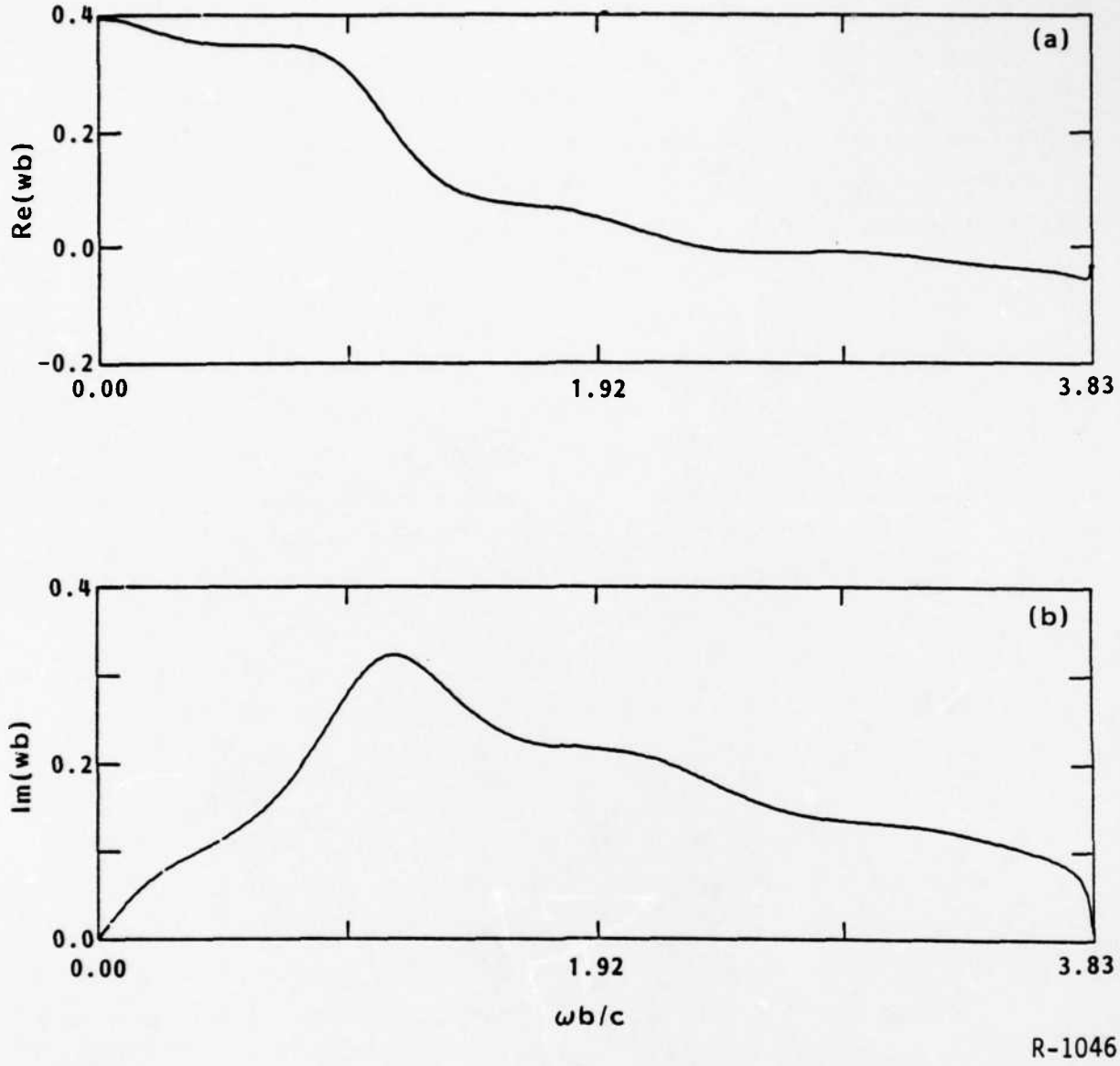

FIGURE 8. REAL (a) AND IMAGINARY (b) PARTS OF NORMALIZED WAKE POTENTIAL FOR RADIAL LINE WITH $R/b = 3.6$, $d/b = 0.1$, AND $Z_s = 1$.

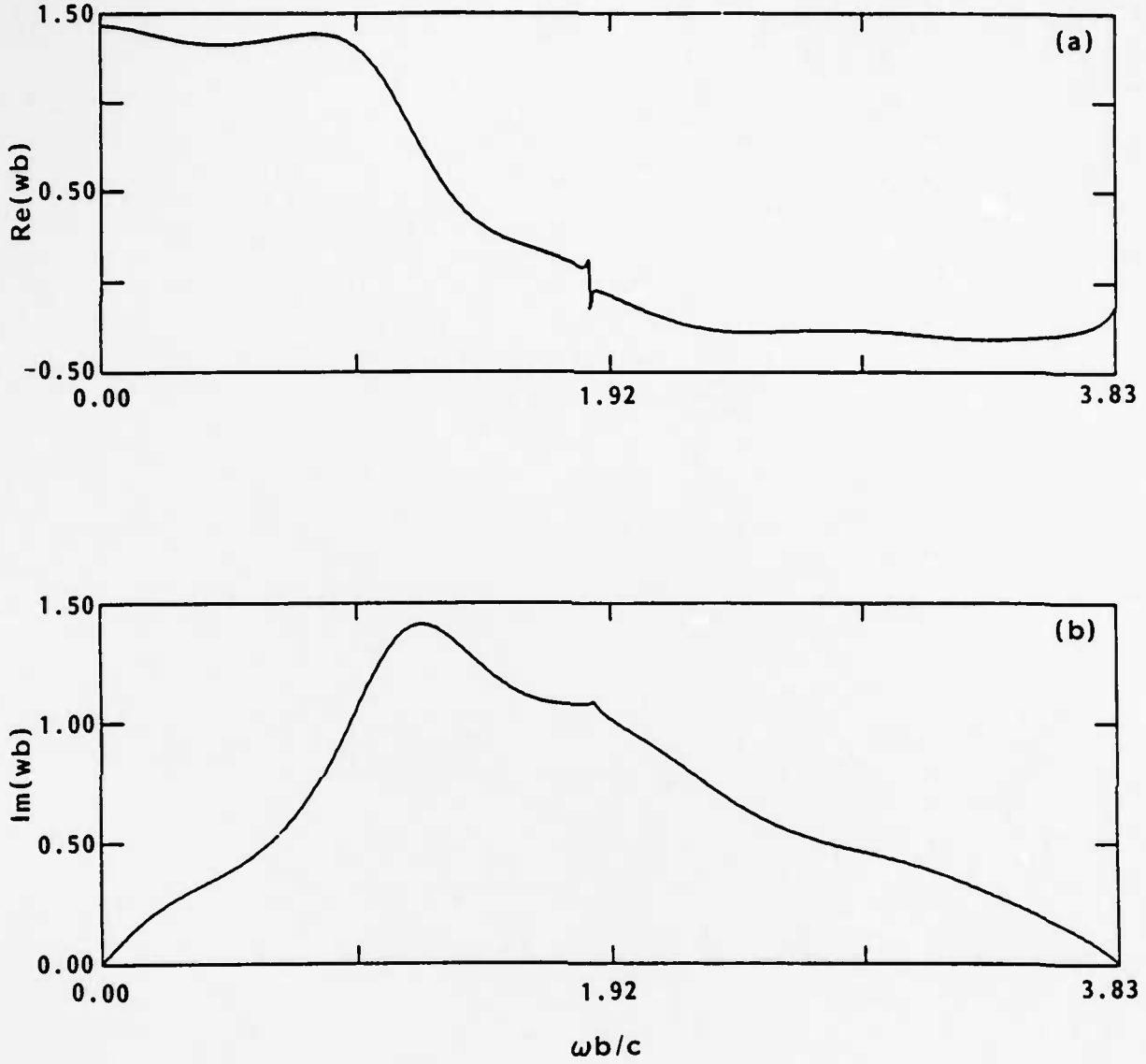

FIGURE 9. REAL (a) AND IMAGINARY (b) PARTS OF NORMALIZED WAKE POTENTIAL FOR RADIAL LINE WITH $R/b = 3.6$, $d/b = 0.5$, AND $Z_s = 1$.

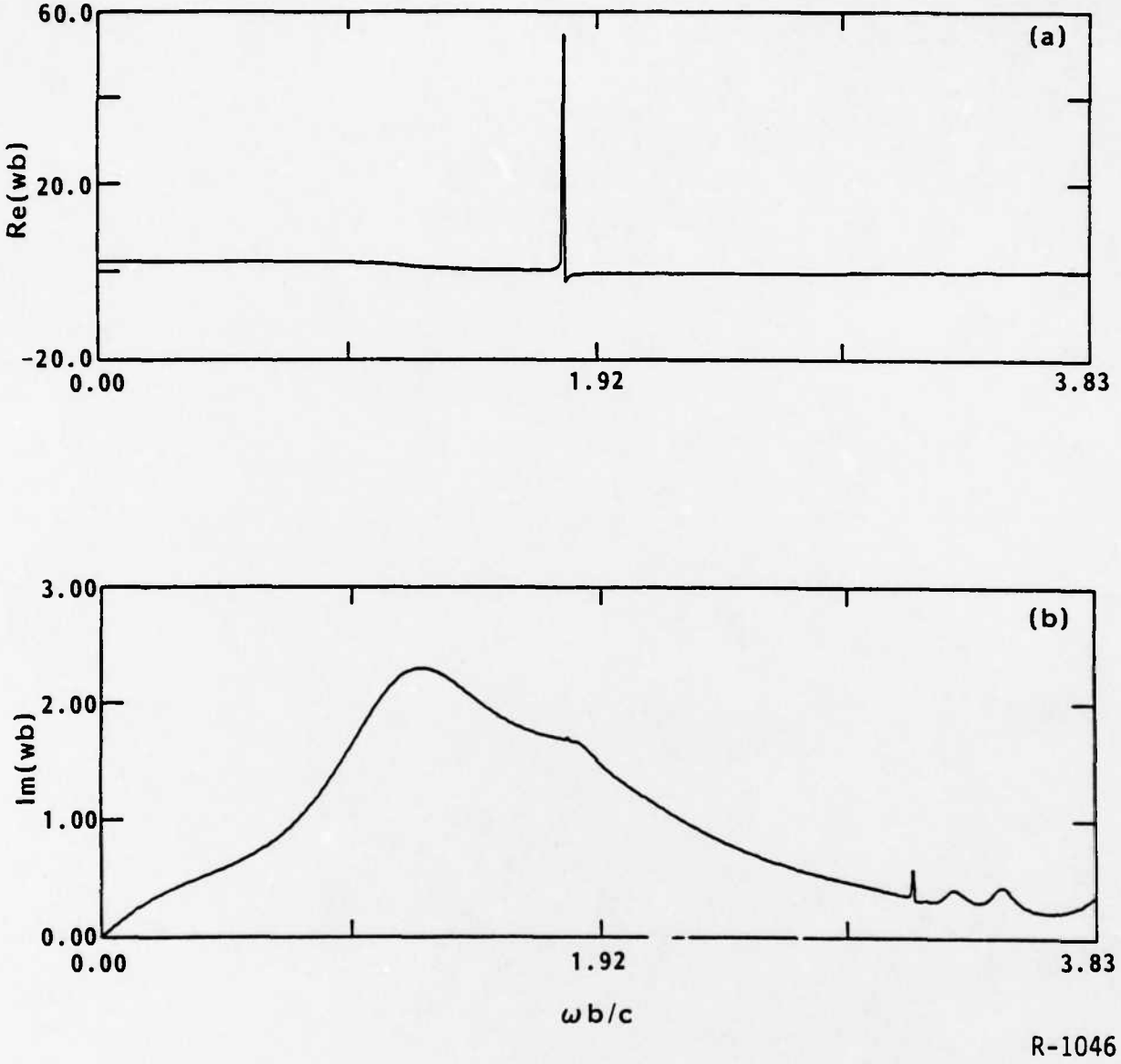

FIGURE 10. REAL (a) AND IMAGINARY (b) PARTS OF NORMALIZED WAKE POTENTIAL FOR RADIAL LINE WITH $R/b = 3.6$, $d/b = 1.0$, AND $Z_s = 1$.

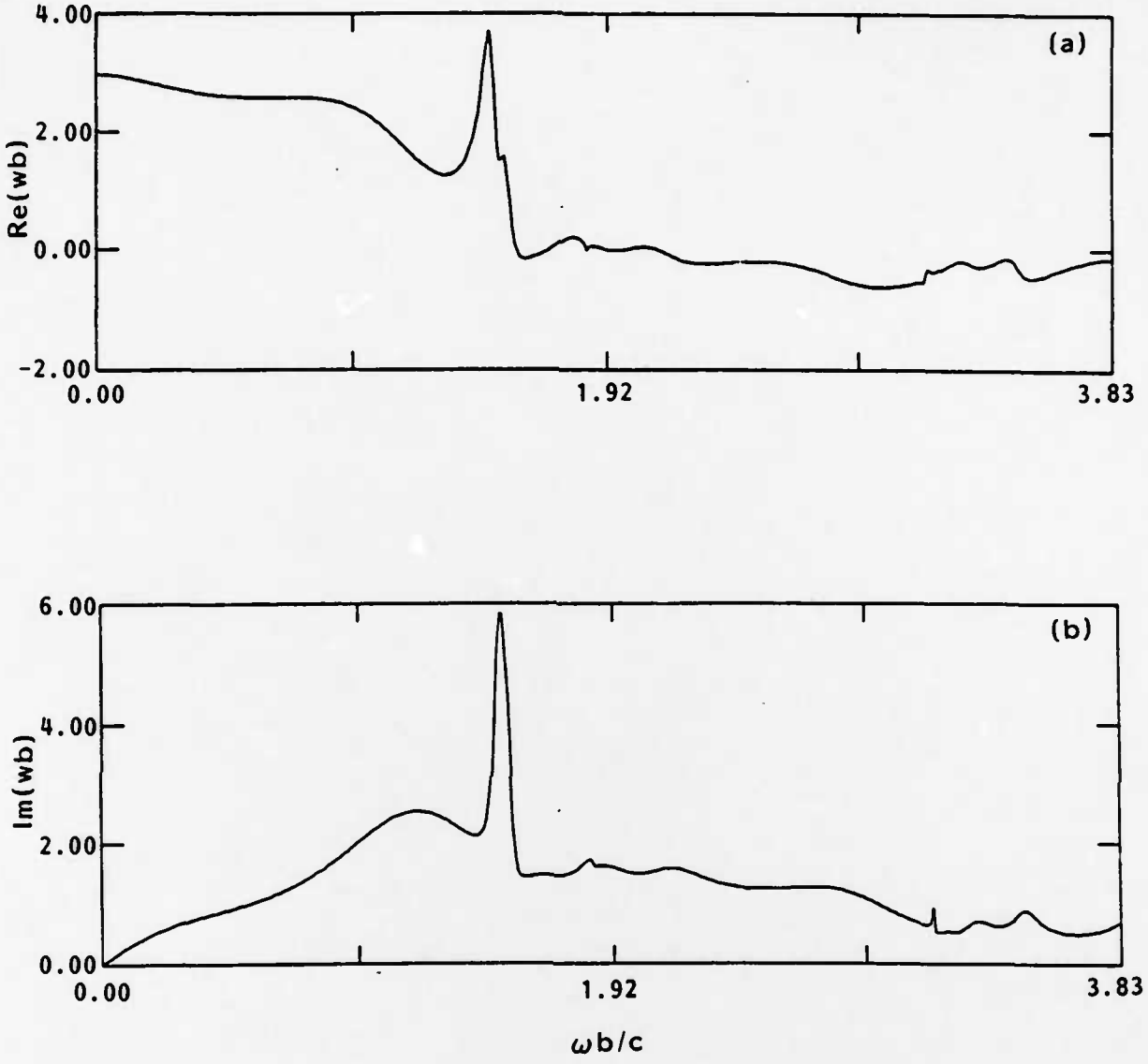

FIGURE 11. REAL (a) AND IMAGINARY (b) PARTS OF NORMALIZED WAKE POTENTIAL FOR RADIAL LINE WITH $R/b = 3.6$, $d/b = 2.0$, AND $Z_s = 1$.

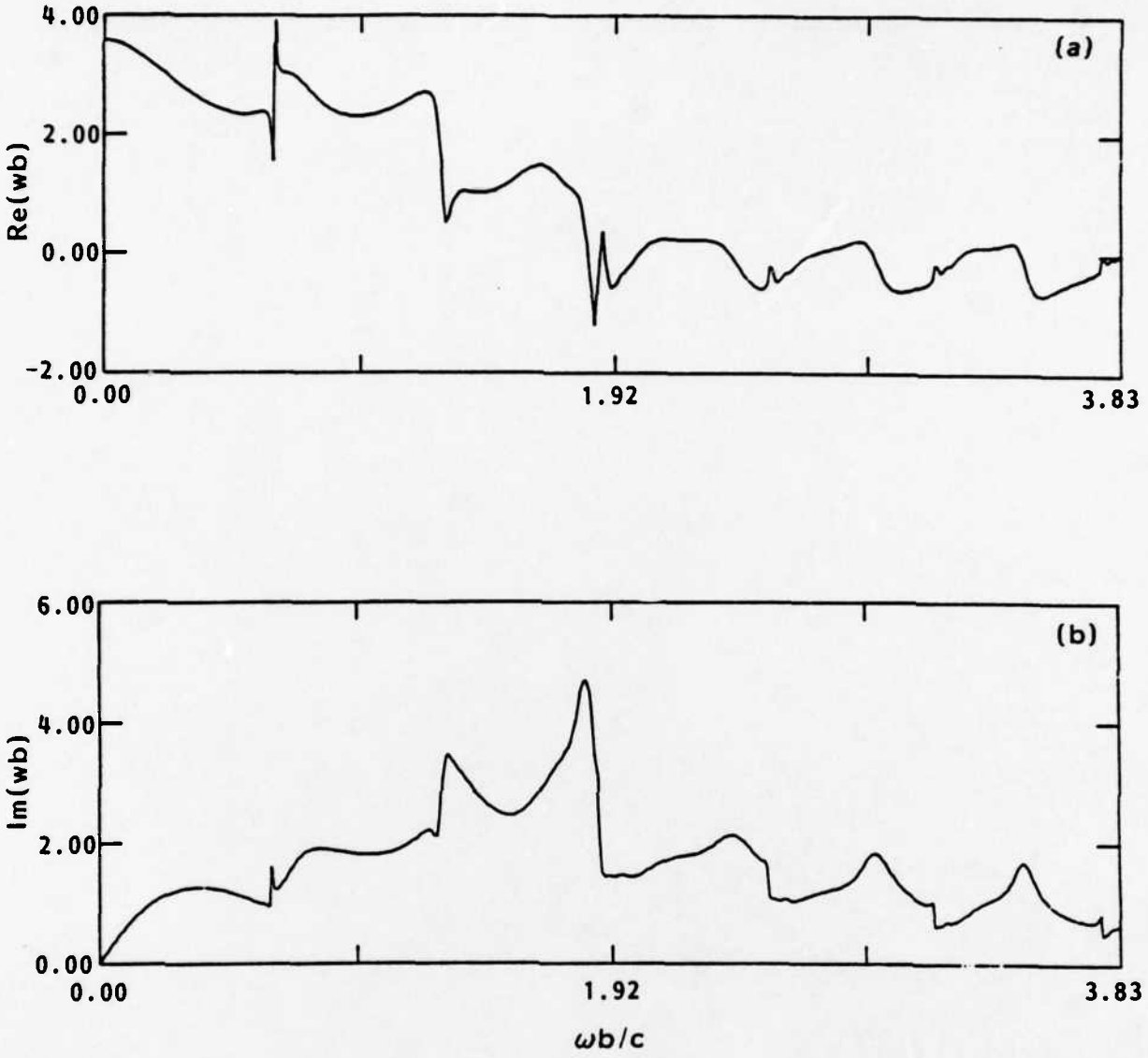

FIGURE 12. REAL (a) AND IMAGINARY (b) PARTS OF NORMALIZED WAKE POTENTIAL FOR RADIAL LINE WITH $R/b = 3.6$, $d/b = 5.0$, AND $Z_e = 1$.

the wave is essentially undamped, because it is just below the TE cutoff and also does not penetrate far enough into the radial line to interact with the termination impedance. In other words, changing Z_s has negligible effect. Mathematically, the resonance arises from the vanishing of the overall determinant of Equations 28–29 and not from an approximate singularity in a single term. Just how narrow the resonance is can be seen from Figure 13, which still has inadequate resolution.

The primary consequence of increasing R/b is to reduce the frequency spacing of modes in the radial line. It also increases the magnitude of the wake potential slightly until R/b exceeds about five. This latter effect is visible but small in Figure 14, $R/b = 10$ when compared with Figure 9, both with $Z_s = 1$. Thus, the length of the radial line is unimportant for an optimal termination impedance. The observation made above that the mode with highest transverse impedance usually lies just below the TE cutoff is well illustrated in Figure 15 for $R/b = 10$ and $Z_s = 0.1$. The wake potential curve becomes very complicated for large R/b and large d/b but still follows the general trends already enumerated.

Some more complicated induction module designs have an enlarged drift tube radius where the transmission line enters. Although complex gap geometries can be treated correctly only with finite-difference field solvers, some insight into those modes due to the expanded drift tube itself can be obtained from the present analysis. Figure 16 is the wake potential of a short, shallow, expanded region with $d/b = 1.0$ and $R/b = 1.5$. A weak resistivity, $Z_s = 10^{-3}$ is applied to the wall at $r = R$. Once again, the mode occurring in the mouth of the gap is present just below the TE cutoff. A heavily damped, probably predominantly TE, mode can be seen near $\omega b/c = 2.6$. Many more modes are introduced by extending the length of the expanded region. See Figure 17 for $d/b = 10$. Of course, transverse impedances and, in some cases, Q's are reduced by employing a less abrupt change in drift tube radius. On general grounds we expect that impedances should decrease by a factor of order $c/\omega\Delta z$ when the drift tube radius changes smoothly over a distance Δz. Nonetheless, more detailed computations indicate that residual transverse impedances are not necessarily negligible.[10]

Implicit in our analysis is the assumption that waves above cutoff in the drift tube propagate only away from the radial line. Real induction accelerators, of course, have many radial feed lines, and power radiated from one may couple to another. Henke has

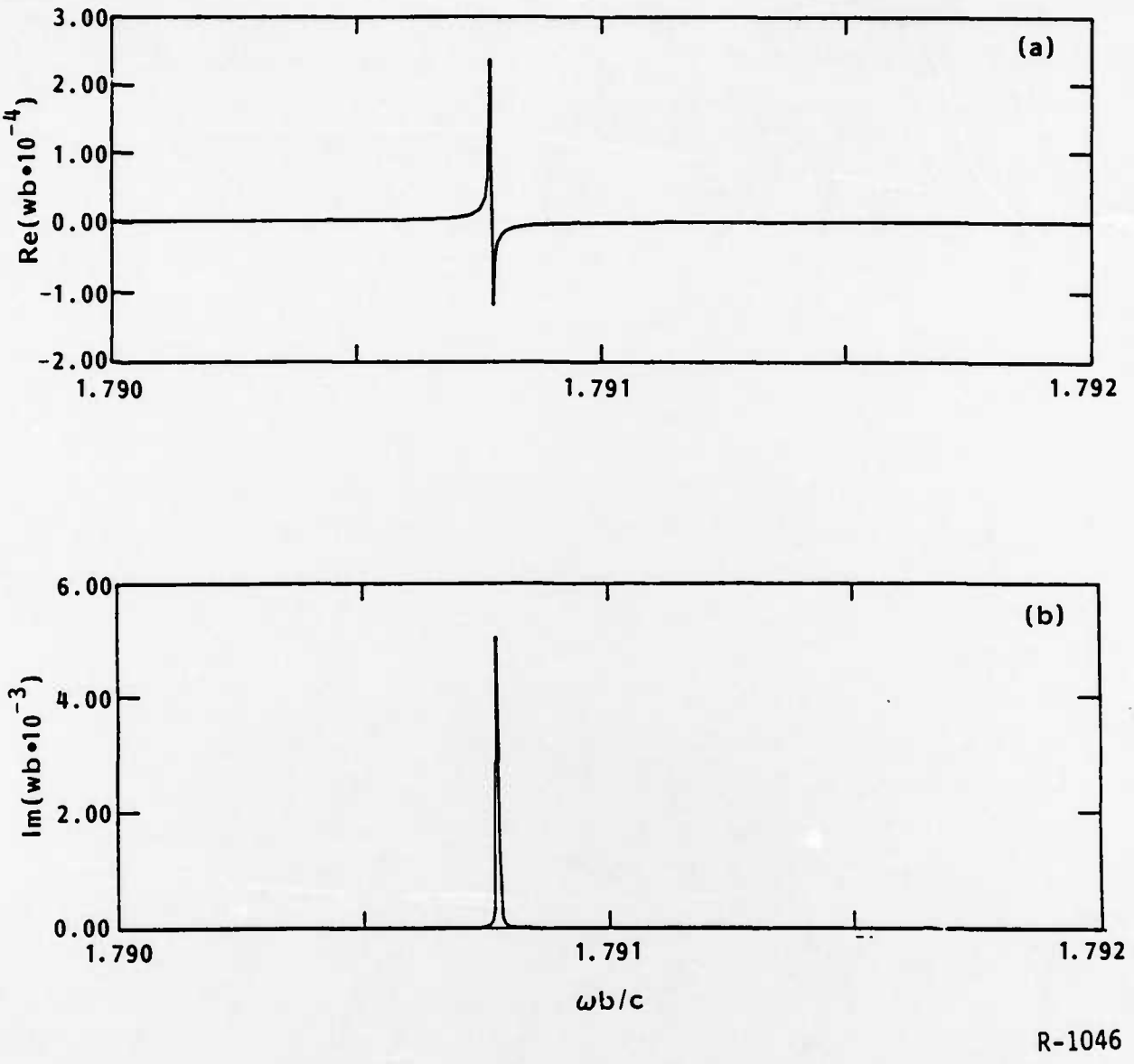

FIGURE 13. THE NORMALIZED WAKE POTENTIAL OF FIGURE 10, HIGHLY RESOLVED IN THE FREQUENCY RANGE $1.790 < \omega b/c < 1.792$.

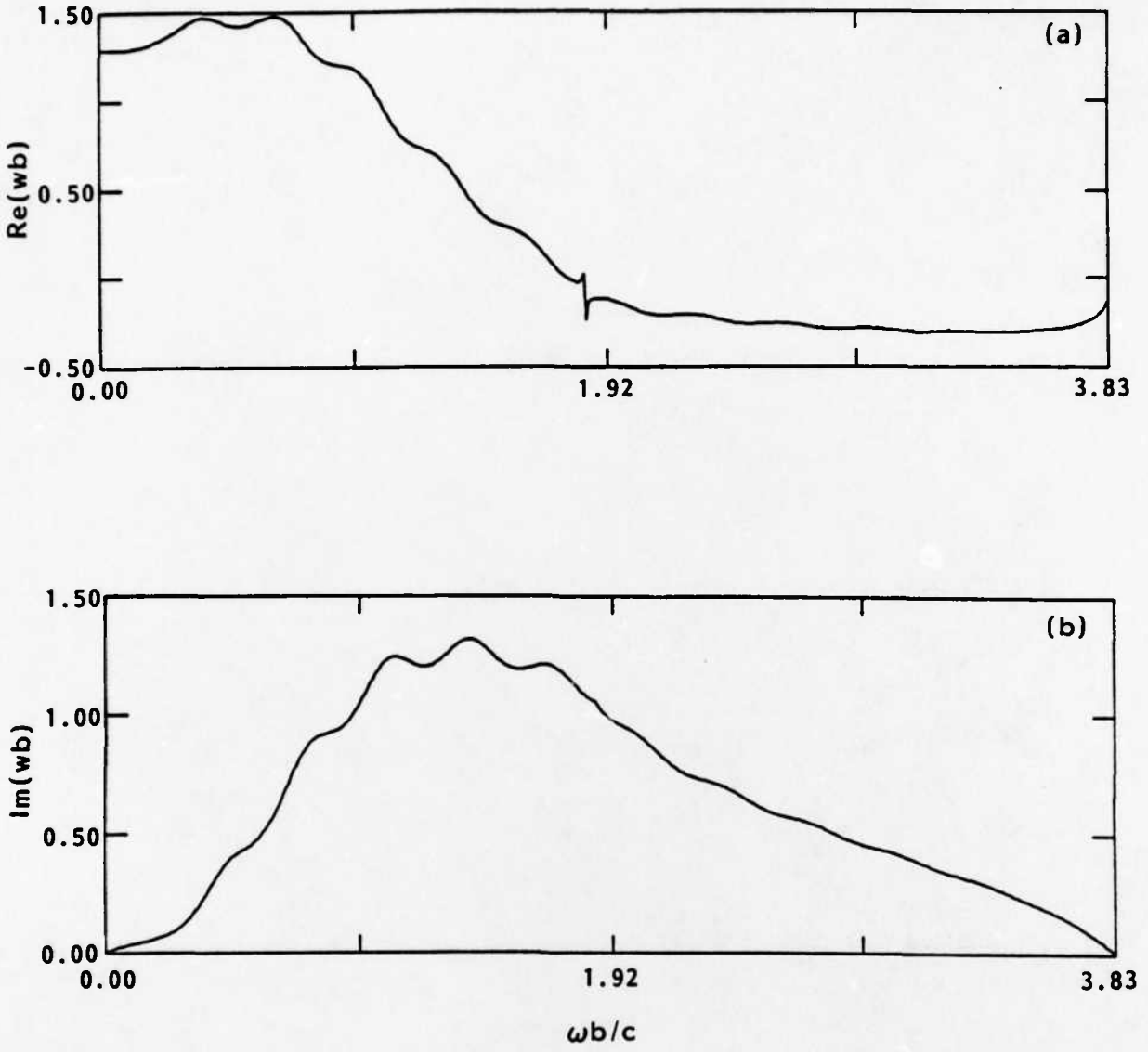

FIGURE 14. REAL (a) AND IMAGINARY (b) PARTS OF NORMALIZED WAKE POTENTIAL FOR RADIAL LINE WITH $R/b = 10.0$, $d/b = 0.5$, AND $Z_s = 1$.

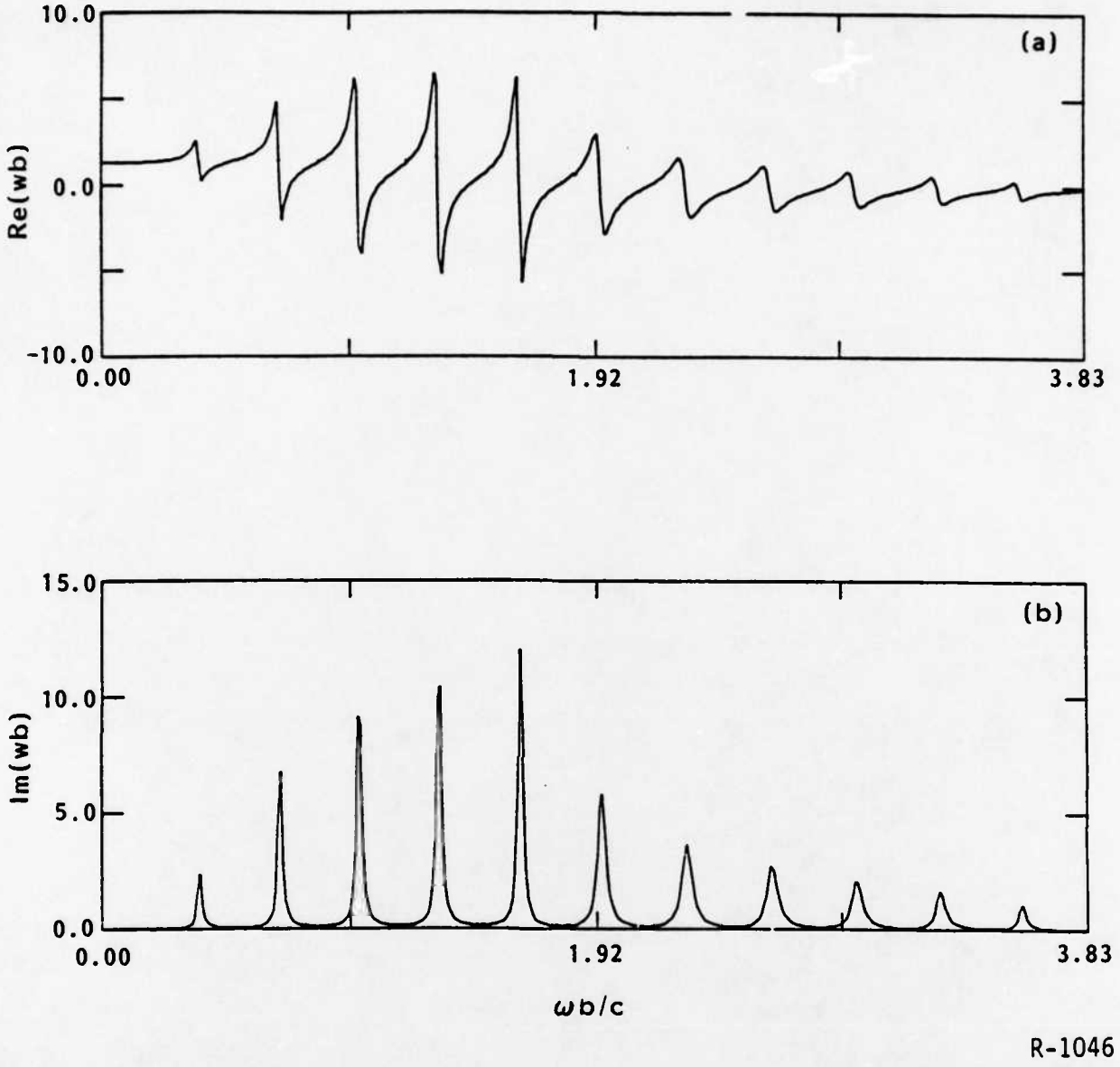

FIGURE 15. REAL (a) AND IMAGINARY (b) PARTS OF NORMALIZED WAKE POTENTIAL FOR RADIAL LINE WITH $R/b = 10.0$, $d/b = 0.5$, AND $Z_s = 0.1$.

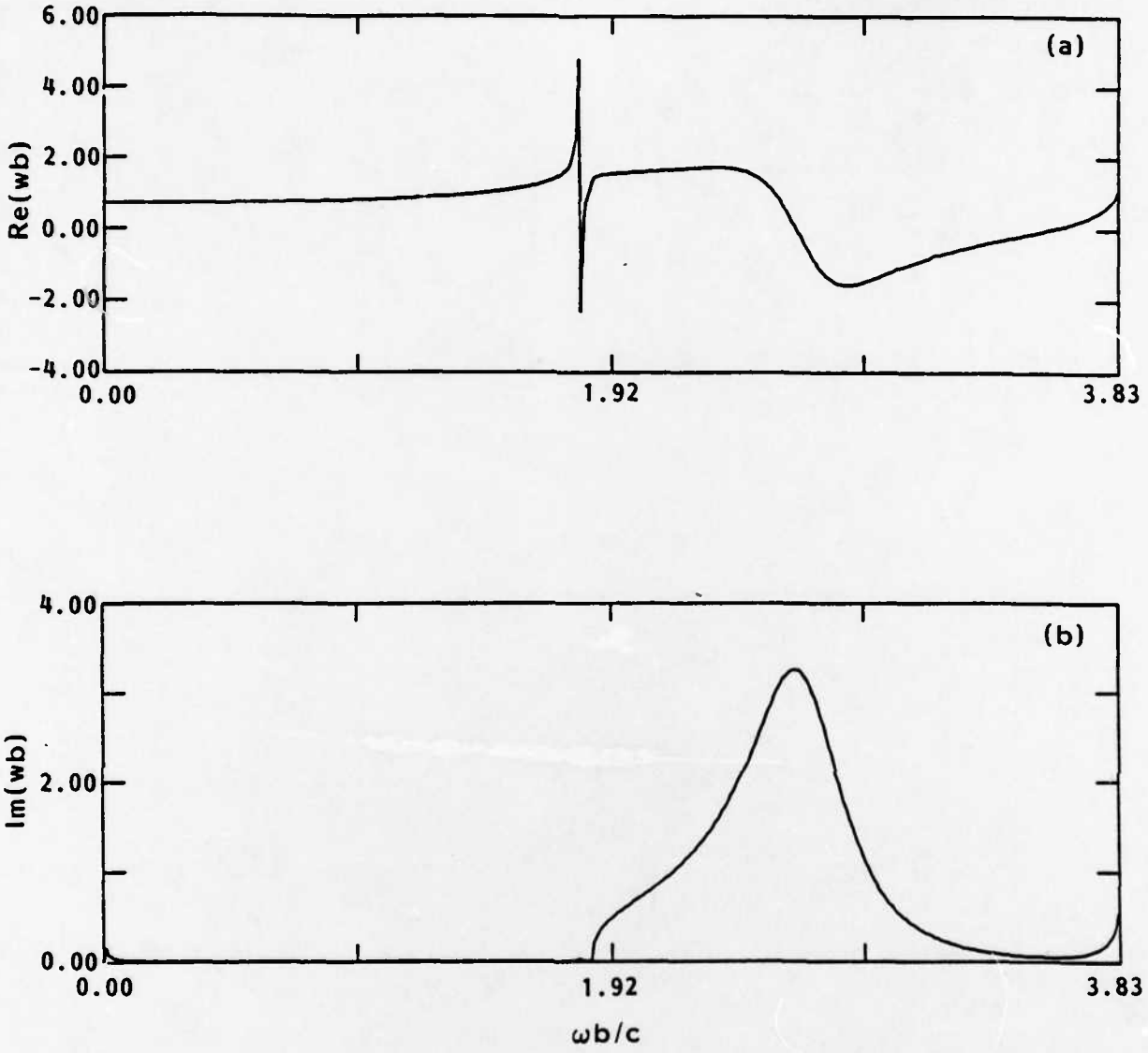

FIGURE 16. REAL (a) AND IMAGINARY (b) PARTS OF NORMALIZED WAKE POTENTIAL FOR SHALLOW RADIAL LINE WITH $R/b = 1.5$, $d/b = 1.0$, AND $Z_s = 0.001$.

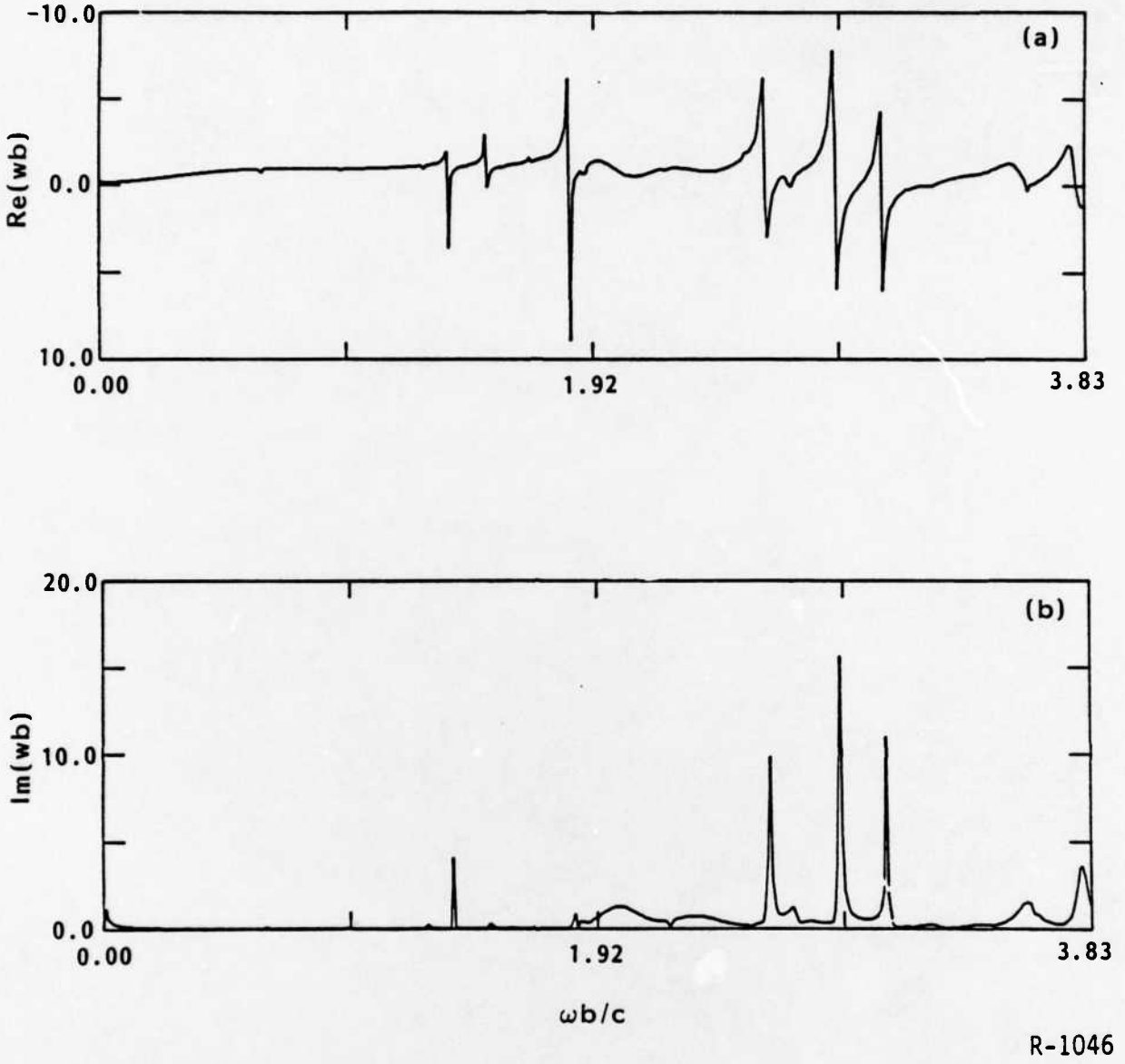

FIGURE 17. REAL (a) AND IMAGINARY (b) PARTS OF NORMALIZED WAKE POTENTIAL FOR SHALLOW RADIAL LINE WITH $R/b = 1.5$, $d/b = 10$, AND $Z_s = 0.001$.

attempted to address this issue by evaluating the overall wake potential of a regularly spaced set of radial lines.[18] However, his analysis is appropriate only for many lines per betatron wavelength, which is not the case in high current electron devices.

We have used the admittedly artificial approach of reversing the sign of the drift tube power flow (i.e., using the positive branch of the square root function when determining complex χ_j in Equations 28 and 29) to obtain a qualitative estimate of the change in wake potential due to electromagnetic waves traveling from one gap to the next. Little difference is observed for heavily loaded lines with $Z_s \approx 1$, probably because little energy is available for radiation into the drift tube. Enhancement of the wake potential does occur for large and small Z_s, however, especially at frequencies between the TE and TM cutoffs. Figure 18 compares wake potentials with oppositely directed energy flow for $d/b = 0.1$, $R/b = 3.6$, and $Z_s = 10$. Resonances above the TE cutoff, while significantly strengthened, still are smaller than the resonance just below the cutoff. It is possible to find worse cases, where $Im(W \cdot b)$ actually becomes negative, perhaps implying absolute instability. However, for most parameters examined the increased transverse impedance does not seem serious. If $m = 1$ electromagnetic coupling of radial lines does prove to be an issue, assuring that the beam wave (i.e., betatron) phase change from gap to gap is different by $\pi/2$ or so from the electromagnetic wave phase change should greatly ameliorate any problems.

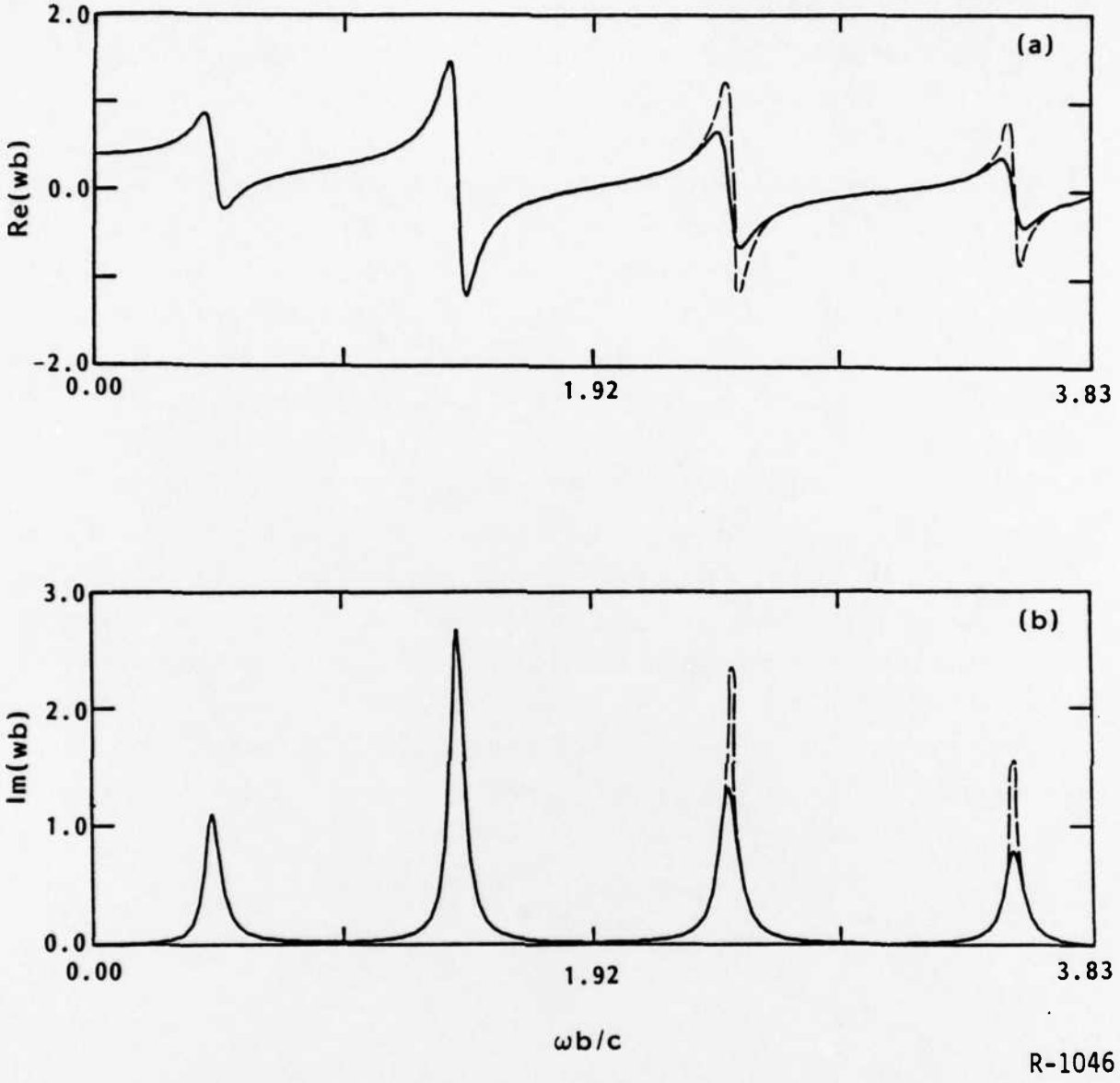

FIGURE 18. REAL (a) AND IMAGINARY (b) PARTS OF NORMALIZED WAKE POTENTIAL FOR RADIAL LINE WITH $R/b = 3.6$, $d/b = 0.1$, AND $Z_s = 10$. DASHED CURVES INDICATE THE EFFECT OF REVERSING THE DIRECTION OF ENERGY FLOW IN THE DRIFT TUBE.

4.0 CONCLUSIONS

The formula for the transverse wake potential associated with a radial line of arbitrary width terminated by a lumped impedance has been derived and evaluated numerically for many sets of parameter similar to those of ATA. Several of the conclusions inferred from the numerical survey are listed at the beginning of Chapter 3. Most important is the finding that the wake potential scales roughly as $1/b$ for $d/b > 1$ instead of d/b^2, the narrow gap result. This new scaling may largely solve the beam breakup instability problem for compact induction accelerators, if pulse power considerations permit wide, well damped, high voltage radial lines. For instance, a 100 MeV Spiral Line Induction Accelerator[7] design with $I = 10$ kA, $B_z = 10$ kG, $b = 3$ cm, and 50 2-MeV lines with $Z_s = 1$ and $d/b = 8/3$ is predicted to have only about three e-foldings of the beam breakup and image displacement instabilities combined.[10]

The reduction of beam breakup growth with gap width is not monotonic, however. Additional modes develop in the radial line as d/b is increased. Several of the figures presented above show a low impedance, high Q mode at $\omega b/c \approx 1.8$ for $d/b \approx 1$. Still more new modes appear for $\omega b/c > \pi b/d$, and their effect on beam breakup can be catastrophic. For instance, if the 50 2-MeV, $d/b = 8/3$ lines of the preceding example are replaced by 100 1-MeV, $d/b = 4/3$ lines, instability growth jumps by two orders of magnitude due to such a weakly damped resonance.[10] It is important, therefore, to carefully analyze and then perform cold tests on proposed radial line designs to assure that strong resonances are avoided.

It is worth remarking that $Z_s = 1$ is not absolutely essential for beam breakup suppression. If, instead, the $Z_s \approx 2$ achieved in ATA[2] is the best that can be obtained in practice, then employing two sets of radial lines with interlaced resonances may be equally effective, because frequencies that grow at one set of radial lines would not grow much at the other.[5] This trick of using different sets of radial lines cannot be extended to more than a few sets, however, because the low-Q modes soon begin to overlap.[21] Cost also is a consideration.

5.0 REFERENCES

1. Caporaso, G. J., Cole, A. G., and Struve, K. W., "Beam Breakup Instability Experiments on ETA and Predictions for ATA," IEEE Trans. Nuc. Sci., Vol. NS-30, 1983, p. 2507.

2. Briggs, R. J., Birx, D. L., Caporaso, G. J., Neil, V. K., and Genoni, T. C., "Theoretical and Experimental Investigation of the Interaction Impedances and Q Values of the Accelerating Cells in the Advanced Test Accelerator," Part. Accel., Vol. 18, 1985, p. 41.

3. Prono, D. S., "Recent Progress of the Advanced Test Accelerator," IEEE Trans. Nuc. Sci., Vol. NS-32, 1985, p. 3144.

4. Caporaso, G. J., Rainer, F., Martin, W. E., Prono, D. S., and Cole, A. G., "Laser Guiding of Electron Beams in the Advanced Test Accelerator," Phys. Rev. Lett., Vol. 57, 1986, p. 1591.

5. Neil, V. K., Hall, L. S., and Cooper, R. K., "Further Theoretical Studies of the Beam Breakup Instability," Part. Accel., Vol. 9, 1979, p. 213.

6. Neil, V. K., The Image Displacement Effect in Linear Induction Accelerators, UCID-17976, Lawrence Livermore National Laboratory, Livermore, CA, 1978.

7. Mondelli, A., Chernin, D., Putnam, S. D., Schlitt, L., and Bailey, V., "A Strong-Focused Spiral-Line Recirculating Induction Accelerator," Beams '86, Osaka University, Japan, 1986.

8. Adler, R., Campbell, M., Godfrey, B., Sullivan, D., and Genoni, T., "Image Displacement Effect in Intense Electron Beams," Part. Accel., Vol. 13, 1983, p. 25.

9. Genoni, T. C., "The Image Displacement Effect," unpublished, 1981.

10. Hughes, T. P. and Godfrey, B. B., Electron Beam Stability in Compact Recirculating Accelerators, MRC/ABQ-R-1040, Mission Research Corporation, Albuquerque, NM, 1988.

11. Weiland, T., "Comment on Wake Field Computation in Time Domain," Nuc. Inst. Meth., Vol. 216, 1983, p. 31.

12. Henke, H., Electromagnetic Interaction between Charged-Particle Beams and Environment, CERN-LEP-RF/86-21, European Organization for Nuclear Research, Geneva, 1986.

13. Henke, H., "Charge Passing Off-Axis through a Cylindrical Resonator with Beam Pipes," IEEE Trans. Nuc. Sci., Vol. NS-32, 1985, p. 2335; presented in expanded form in Point Charge Passing through a Resonator with Beam Pipes, CERN-LEP-RF/85-41, European Organization for Nuclear Research, Geneva, 1986.

14. Jackson, J. D., Classical Electrodynamics, Wiley, New York, NY, 1966, pp. 241-242.

15. Abramowitz, M. and Stegun, I. A., Handbook of Mathematical Functions, U. S. Government Printing Office, Washington, DC, 1965, Sec. 9, pp. 358-373.

16. Weiland, T., "Transverse Beam Cavity Interaction," Nuc. Inst. Meth., Vol. 212, 1983, p. 31.

17. Dongarra, J. J., Moler, C. B., Bunch, J. R. and Stewart, G. Q., LINPACK Users' Guide, Society for Industrial and Applied Mathematics, Philadelphia, 1979, Ch. 1.

18. Henke, H., Impedances of a Set of Cylindrical Resonators with Beam Pipes, CERN-LEP-RF/87-62, European Organization for Nuclear Research, Geneva, 1987.

19. Caporaso, G. J., unpublished.

20. Morse, P. M. and Feshbach, H., Methods of Theoretical Physics, McGraw-Hill, New York, NY, 1953, Vol. I, pp. 449-451.

21. Godfrey, B. B. and Miller, R. B., unpublished.

DTIC

4-89

END

DATE

FILMED